Spatial Interactions in the Superior Colliculus Predict Saccade Behavior in a Neural Field Model

Robert A. Marino[1], Thomas P. Trappenberg[2], Michael Dorris[1], and Douglas P. Munoz[1]

Abstract

■ During natural vision, eye movements are dynamically controlled by the combinations of goal-related top–down (TD) and stimulus-related bottom–up (BU) neural signals that map onto objects or locations of interest in the visual world. In primates, both BU and TD signals converge in many areas of the brain, including the intermediate layers of the superior colliculus (SCi), a midbrain structure that contains a retinotopically coded map for saccades. How TD and BU signals combine or interact within the SCi map to influence saccades remains poorly understood and actively debated. It has been proposed that winner-take-all competition between these signals occurs dynamically within this map to determine the next location for gaze. Here, we examine how TD and BU signals interact spatially within an artificial two-dimensional dynamic winner-take-all neural field model of the SCi to influence saccadic RT (SRT). We measured point images (spatially organized population activity on the SC map) physiologically to inform the TD and BU model parameters. In this model, TD and BU signals interacted nonlinearly within the SCi map to influence SRT via changes to the (1) spatial size or extent of individual signals, (2) peak magnitude of individual signals, (3) total number of competing signals, and (4) the total spatial separation between signals in the visual field. This model reproduced previous behavioral studies of TD and BU influences on SRT and accounted for multiple inconsistencies between them. This is achieved by demonstrating how, under different experimental conditions, the spatial interactions of TD and BU signals can lead to either increases or decreases in SRT. Our results suggest that dynamic winner-take-all modeling with local excitation and distal inhibition in two dimensions accurately reflects both the physiological activity within the SCi map and the behavioral changes in SRT that result from BU and TD manipulations. ■

INTRODUCTION

The spatial organization of the external world is represented in neural maps throughout the visual system (Hall & Moschovakis, 2003; Kaas, 1997; Cynader & Berman, 1972; Hubel & Wiesel, 1969). For primates, these maps are especially important because the highest visual acuity is limited to the fovea wherein only 1–2° of visual angle are represented (Perry & Cowey, 1985). Because the fovea can only be at one place at any time, simultaneously occurring relevant or interesting objects in the visual field must compete for foveation. The two neural processes that influence saccades are stimulus-triggered bottom–up (BU) and goal-directed top–down (TD; Fecteau & Munoz, 2006; Itti, Rees, & Tsotsos, 2005). BU processes reflect the exogeneous properties of external visual stimuli. TD processes involve endogeneous, internally driven cognitive mechanisms that reflect the relevancy of task-driven goals. In the oculomotor system, how TD and BU signals are combined in neural maps to influence saccade processing is poorly understood. The goal of this study is to develop a two-dimensional neural field model of the intermediate layers of the superior colliculus (SCi) that is constrained by new physiological data and is capable of explaining how TD and BU processes interact and compete to account for observed saccade behavior.

The SCi is the ideal place in which to model these relationships because it is a critical structure in the guidance of saccadic eye movements (Schiller, Sandell, & Maunsell, 1987; Schiller, True, & Conway, 1980). The SCi contains a map that has been described physiologically (Robinson, 1972) and defined mathematically (Van Gisbergen, Van Opstal, & Tax, 1987; Ottes, Van Gisbergen, & Eggermont, 1986). The SCi also serves as a sensorimotor integration node where sensory (Meredith & Stein, 1985; Goldberg & Wurtz, 1972), saccadic preparation (Basso & Wurtz, 1998; Dorris & Munoz, 1998), and saccadic motor signals (Munoz & Wurtz, 1995a; Sparks & Mays, 1980; Sparks, 1978) converge onto individual neurons that are spatially aligned within the visual field (Marino, Rodgers, Levy, & Munoz, 2008) and project directly to the premotor circuitry in the brainstem to drive saccades (Rodgers, Munoz, Scott, & Pare, 2006; Scudder, Moschovakis, Karabelas, & Highstein, 1996; Moschovakis, Karabelas, & Highstein, 1988).

[1]Queen's University, Kingston, Canada, [2]Dalhousie University, Halifax, Canada

Recent evidence suggests that lateral interactions contribute to the spatial interactions of activity within the SCi map. These interactions can result in local regions of excitation and surrounding regions of remote inhibition on the SCi map (Figure 1A; Dorris, Olivier, & Munoz, 2007). When multiple BU and TD signals arrive in the SCi, physiological evidence has suggested that a single saccadic goal is selected via a winner-take-all mechanism (Dorris et al., 2007; McPeek & Keller, 2002; Munoz & Fecteau, 2002; Trappenberg, Dorris, Munoz, & Klein, 2001; Munoz & Istvan, 1998). Neural field models of the oculomotor system employing such lateral interactions (Amari, 1977) have been shown to accurately simulate saccadic behavior (Wang, Jin, & Jabri, 2002) across several task conditions (Kopecz, 1995; Kopecz & Schoner, 1995). When specifically applied to describe the activity within the SC, this type of model has been able to successfully account for an even larger variety of saccadic behaviors, including (1) differences in saccadic RT (SRT) because of endogeneously and exogeneously triggered saccades (Trappenberg, 2008; Trappenberg et al., 2001), (2) saccade trajectory variations produced by focal SCi lesions (Badler & Keller, 2002), and (3) competing visual stimuli (Arai & Keller, 2005).

Here, we present a general competitive interaction model that has been constrained by known SC physiology. Although our model makes the assumption that the spatial interactions that influence saccadic decisions are being computed at the level of the SC, it does not preclude the possibility that these computations could be occurring by or in conjunction with other structures in the oculomotor system and then relayed to the SC. Here, we are simply exploring the possible consequences of these interactions within the local SC circuitry.

The model presented here extends an earlier model (Trappenberg et al., 2001) by addressing several limitations of the previous one-dimensional architecture that was not reflective of the two-dimensional neural map represented within the SC (Robinson, 1972). By expanding the model into two dimensions, we can incorporate more physiological details of the spatial organization of saccade-related activity. Although similar spatial interaction mechanisms can be demonstrated within the previous one-dimensional model, scaling up to two dimensions allows for a greater number of saccade-related signals to be simulated across the visual field. Only a two-dimensional model is capable of accurately recreating and simulating experiments wherein more than two equally distant BU or TD saccade-related signals are presented around the fovea.

Furthermore, the spatial sizes of the TD and BU input parameters in this previous model were only roughly estimated from individual neural response fields (Munoz & Wurtz, 1995a, 1995b). A more accurate estimate of these spatial parameters should reflect the population activity or "point image" (McIlwain, 1986; spatially organized regions of localized activity on the SC map). This is critical because individual response fields show significant variation in both size and magnitude, whereas point images remain approximately constant across the SC map for different target locations and saccade vectors (Marino et al., 2008; Anderson, Keller, Gandhi, & Das, 1998; Munoz & Wurtz, 1995b).

The neural mechanisms that underlie how TD and BU processes influence saccades are poorly understood, yet they have a profound effect on the timing or "mental chronometry" (Posner, 2005) of the sensory to motor transformations that are computed by the visual and oculomotor systems. Previous RT studies on the effects of TD target predictability and BU stimulus intensity and numbers of stimuli show many apparent inconsistencies and contradictions that seem to indicate that the underlying neural mechanisms are highly complex. However, we demonstrate here that lateral interactions within a winner-take-all model of the SCi can account for these many different results via the simple spatial properties and locations of the underlying TD and BU point images in the SCi (Figure 1).

To improve the physiological accuracy of the model, we measure the point images of BU sensory responses and pretarget TD preparatory responses in the SCi and used them to constrain the input parameters in the model. Then, we model how the spatial interactions between TD or BU signals can influence SRT. We test how these interactions can occur both within individual signals at a single location (i.e., via changes in magnitude and width; Figure 1B) or between multiple signals at different locations in the map (Figure 1C). Specifically, we assess how SRT is influenced by the (1) area of tissue activated (Figure 1B), (2) peak magnitude of the input signal, (3) distance between input signals (Figure 1C), and (4) overall number of competing TD or BU signals. When only one TD or BU input signal is present within the model, we hypothesize that signals that extend beyond the area of local excitation in the SC map will trigger saccades more slowly than narrower input signals (Figure 1B). This may result because signals with wider activation than the excitatory interaction region could simultaneously activate both local excitatory and remote inhibitory connections (Munoz & Istvan, 1998). This should increase accumulation time to saccadic threshold leading to an increase in SRT. When two or more input signals are present, we hypothesize that distal signals will mutually inhibit each other and result in slower SRTs while simultaneously occurring proximal signals will combine their point images (activity on the SC map) and lead to faster SRT (Figure 1C).

METHODS

Animal Preparation

All animal care and experimental procedures were in accordance with the Canadian Council on Animal Care

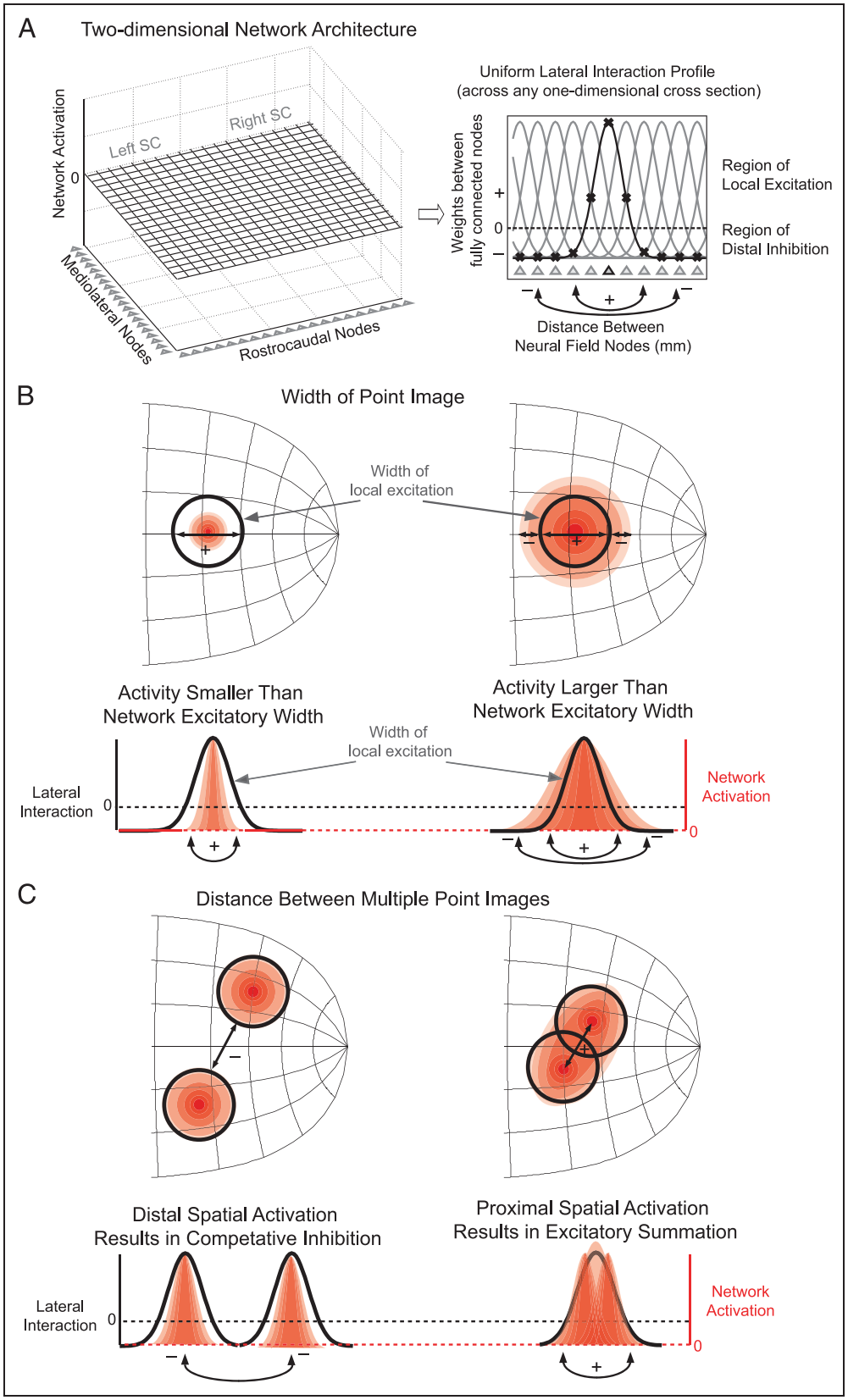

Figure 1. (A) Left: Architecture of the two-dimensional neurofield model (developed from Trappenberg et al., 2001). Right: Schematic of the Gaussian-shaped spatial profile of local excitation and distal inhibition centered at each neural node within the model. (B and C) Schematics of spatial competition and lateral interaction that can occur from individual (B) or multiple (C) activation signals within the retinotopic, topographical SCi map as predicted by our model. (B) Lateral interaction could theoretically result from individual hills of activity corresponding to spatially specific TD or BU signals, depending on whether they are wider (right) or narrower (left) than the underlying excitatory interaction profile in the SCi map. Spatial signals that are wider than the width of the excitatory area will result in lateral inhibition across the input signal. This lateral inhibition is predicted to result in longer SRT relative to spatial signals whose width does not exceed the width of local excitation. (C) When input signals (either TD or BU) are distant, dynamic winner-take-all mechanisms must resolve the resulting saccade vector by suppressing competing TD and BU signals. In the case where these competing signals are distant, the corresponding spatial signals on the SCi map are distant and spatially distinct. In this case, strong lateral inhibition suppresses each competing signal until only one remains. However, in the case where these competing signals are close together, they could additively combine into a larger area of excitation in the SCi map. We predict that the summation of nearby signals should reduce SRT relative to more distant signals because of the more global area of excitation that results on SCi the map.

policies on use of laboratory animals and approved by Queen's University Animal Care Committee. Four male monkeys (*Macaca mulatta*) were used in these studies. A detailed description of the surgical techniques used to prepare animals for neuronal and eye movement recordings in our laboratory have been described previously (Marino et al., 2008).

Experimental Tasks and Behavioral Stimuli

Neurophysiological experiments were designed to measure BU and TD point images in the SCi. Behavioral paradigms and visual displays were under the control of a UNIX-based real-time data control and presentation systems (Rex 6.1; Hays, Richmond, & Optican, 1982). The display screen spanned ±35° of the central visual field. Luminance was measured with a hand held photometer (Minolta CS-100) that was positioned at the same location as the monkey (86 cm away from the display screen). Monkeys were required to perform several interleaved visually guided saccade tasks, including the delay and gap tasks (e.g., Figure 2A and B), as well as the step task and memory-guided task (paradigms and data not shown). Experiments were performed in total darkness with individual trials lasting ~1–2 sec. Each trial required the monkey to generate a single saccade from the central fixation point (FP) to a peripheral visual target. During the intertrial interval (duration of 800–1500 msec), the display screen was diffusely illuminated to prevent dark adaptation. At the start of each trial, the screen turned black, and after a period of 250 msec, a red FP (0.3 cd/m^2) appeared at the center of the screen against a black background. Following FP appearance, the monkeys had 1000 msec to fixate the FP before the trial was aborted as an error. Central fixation was then maintained for a variable period (500–800 msec) until the target (5 cd/m^2) appeared.

The delay task (Figure 2A) was used to dissociate visual and saccade-related activity. In this task, the monkeys were required to continue fixation of the FP for an additional 500–800 msec after target appearance. Only after FP disappearance was the monkey allowed to initiate a saccade to the target. The trial was scored as an error and analyzed separately if fixation was broken before FP disappearance or if the monkey did not complete a saccade to the target location within a 2° window (of visual arc) around the target or if the monkey failed to initiate a saccade within 1000 msec of FP disappearance. The gap task (Figure 2B) was used to minimize the inhibition resulting from active visual fixation (Krauzlis, 2003; Machado & Rafal, 2000; Paré & Munoz, 1996; Dorris & Munoz, 1995). In the gap task, a 200-msec period of

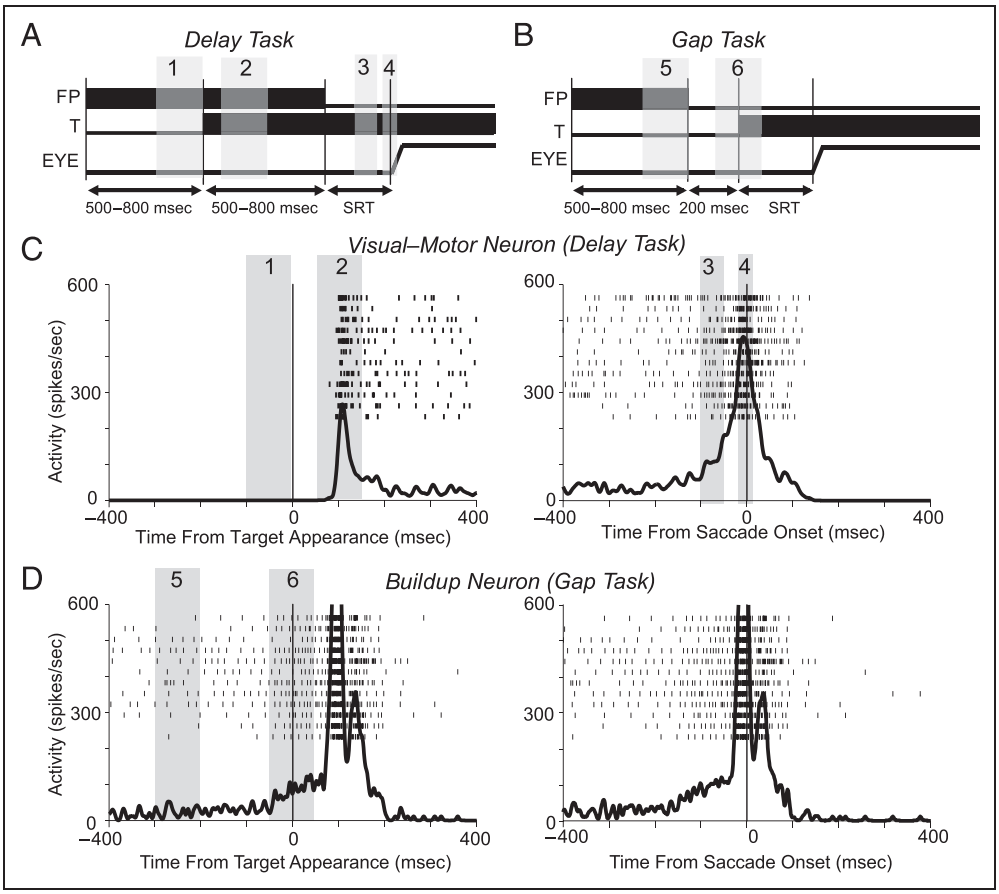

Figure 2. Schematic representation of temporal events in the delay (A) and gap (B) tasks for the FP, target (T) and eye position. Numbered gray bars denote the critical epochs used to classify visual and motor-related activity in the delay task (A) as well as preparatory activity in the gap task (B). Representative neurons from each class aligned on target appearance (left column) and saccade onset (right column). (C) Visual–motor neuron in the delay task. (D) Representative visual–motor neuron with significant pretarget buildup activity in the gap task.

darkness (gap) was inserted between FP disappearance and target appearance (Saslow, 1967). The monkey was required to continue central fixation until target appearance and then initiate a saccade to the target within 1000 msec of its appearance. Tasks were randomly interleaved within two separate blocks of trials. In the first block, targets were presented at one of two possible locations: at the center of each neuron's response field (see below) or opposite the horizontal and vertical meridians. In the second block, the targets were presented at 10° left or right of center along the horizontal meridian. Each correct trial was rewarded with a drop of fruit juice or water. The duration of all correct trials ranged from approximately 1–2 sec, depending on the variability of fixation duration and SRT.

Neural Classification

All techniques for extracellular neuronal recording and data collection were described previously (Dorris et al., 2007). To characterize the activity of individual neurons, trains of action potentials averaged across all correct trials were convolved into spike density functions using a gaussian kernel (σ = 5 msec) for each spike (Richmond, Optican, Podell, & Spitzer, 1987). Spike density functions were aligned on target appearance when analyzing visual responses (Figure 2C and D, left) and saccade onset when analyzing motor responses (Figure 2C and D, right).

We recorded 113 single neurons from four monkeys (see Table 1). The delay task was used to temporally dissociate and classify visual and motor-related activity in all neurons. On the basis of this classification, 106 of 113 neurons had both visual and motor responses (VMBNs) and 7 neurons exhibited only motor responses (MBNs) when the target was centered in each neuron's response field. The gap task was used to subclassify those VMBNs and MBNs that also exhibited buildup activity (BUNs) based on the presence of significant pretarget preparatory activity in the gap period (Dorris, Pare, & Munoz, 1997; Munoz & Wurtz, 1995a). On the basis of this subclassification, 42 of 113 neurons exhibited pretarget buildup activity (of which 35 were VMBNs and 7 were MBNs) and the remaining 71 of 113 VMBNs had no buildup activity.

Visual responses were determined from target-aligned activity in the delay task (50–150 msec after target appearance; Figure 2A, Epoch 2). The last 100 msec of active fixation before target appearance (Figure 2A, Epoch 1) was used to compute a visual baseline threshold, which was then compared with the visual response in Epoch 2. A visual response was defined as a statistically significant increase in target-aligned activity greater than 50 spikes/sec above the visual baseline threshold.

Saccade responses were determined from movement-aligned activity in the delay task (±10 msec around the onset of the saccade; Figure 2A, Epoch 4). Saccade responses were compared with both the visual (Epoch 1) and saccade baseline thresholds (100–50 msec before the onset of the saccade; Figure 2A, Epoch 3). The saccade baseline threshold (Epoch 3) was used to ensure that any sustained tonic visual activity related to the continued presence of the target was not misclassified as motor-related saccade activity. A motor response was defined as a statistically significant increase in saccade-aligned activity that was at least 50 spikes/sec above both the visual and saccade baseline thresholds (Epochs 1 and 3). VMBNs (e.g., Figure 2C) exhibited a significant increase in discharge related to both the appearance of a visual target (visual response) and the initiation of the saccade (motor response). MBNs were similar to VMBNs, except that they did not exhibit a significant visual response.

All subclassified BUNs exhibited a significant increase in their activity (preparatory buildup) during the gap epoch (50 msec before to 50 m after target appearance in the gap task; Figure 2B, Epoch 6) in the gap task. Preparatory buildup activity was defined as a statistically significant increase in discharge between the visual baseline (last 100 msec of active visual fixation in the gap task; Figure 2B, Epoch 5) and the gap epoch (Epoch 6). The gap epoch ended before the onset of the earliest visual responses for all neurons recorded. All significant increases between epochs were determined by a Wilcoxon rank-sum test, $p < .05$.

Table 1. SCi Neuron Breakdown by Monkey and Subtype

Monkey (Age, Weight)	*VMBN (No Buildup)*	*BUN VM*	*BUN M*
F (9 years, 7.2 kg)	40	18	4
H (6 years, 7.5 kg)	21	7	1
O (6 years, 11.6 kg)	10	9	2
R (8 years, 10 kg)	0	1	0
Total neurons	71	35	7

VMBN = visual–motor burst neuron with no buildup activity; BUN = a motor burst neuron with buildup activity that may (BUN-VM) or may not (BUN-M) also exhibit a visual response to the appearance of the target.

Calculation of Neural Population Point Images on the SC Map

We analyzed the population activity or point images (McIlwain, 1975, 1986) of BU visual, TD motor preparation, and saccadic motor activity across the SC during presentation of targets at 10° left and right. The position of each neuron on the map was determined from the saccadic vector within the motor response field that yielded the maximal motor discharge of action potentials at movement onset (Marino et al., 2008). This was determined on-line by systematically testing the motor response to multiple saccade vectors across each cell's motor response field.

To visualize spatial properties within the SC map, visual field coordinates were transformed into SC coordinates using previously described transformations (Van Gisbergen et al., 1987; Ottes et al., 1986),

$$u = B_u \ln\left(\frac{\sqrt{R^2 + 2AR\cos(\Phi) + A^2}}{A}\right) \quad (1)$$

$$v = B_v \arctan\left(\frac{R\sin(\Phi)}{R\cos(\Phi) + A}\right) \quad (2)$$

wherein u denotes the anatomical distance from the rostral pole (mm) along the horizontal position axis, v is the distance (mm) along the vertical axis, R is the retinal eccentricity, and Φ is the meridional direction of the target (°). The constants are $B_u = 1.4$ mm; $B_v = 1.8$ mm/rad; and $A = 3°$. The spatial extent of each point image was calculated from a cubic spline (de Boore, 1978) that interpolated between the cell locations on the SC map. Population point image activity was calculated by plotting all activity ipsilateral to the target stimulus within the left SC and all activity contralateral to the target stimulus within the right SC. Neurons were mirrored across the horizontal meridian to improve the spatial resolution of the fitted surface by exploiting the underlying symmetry within the map. This assumption of symmetry was based upon no observed vertical biases (above or below the horizontal meridian) in visuomotor responses between the upper and lower visual fields when plotted on the SC map beyond 2° eccentricity (Marino et al., 2008; van Opstal & van Gisbergen, 1989).

The BU visual response was calculated from the peak of the isolated visual response recorded from VMBNs in the delay task (peak response occurred 102 msec after target appearance; Figures 3A, left and 4A). It was necessary to calculate the isolated visual response from the delay task instead of the gap task because in the delay task the visual response does not combine with TD preparatory activity and is separated temporally from the saccadic motor response. The TD preparatory response was calculated from the maximum buildup activity of BUNs in the gap task that occurred immediately before the onset of the visual response (which occurred 55 msec following target presentation; Figures 2D, 3B, and 4B). The combined TD and BU response was calculated from all combined VMBNs and BUNs in the gap task immediately after the onset of the visual response, but before the extinction of the preparatory activity that had accumulated at the other possible target location (90 msec following target presentation; Figure 4C). The saccadic motor burst was calculated from all combined VMBNs and BUNs in the gap task at saccade onset. The size of the TD preparatory, BU visual, and motor point images were determined independently using both the half width of the peak activity falling along the horizontal meridian (Figure 4A–D, bottom) and from the standard deviation (σ) of a fitted two-dimensional Gaussian function defined by

$$f(x,y) = Ae^{-\left(\frac{(x-x_o)^2 + (y-y_o)^2}{2\sigma^2}\right)} \quad (3)$$

wherein x_o, y_o, and σ were calculated independently from each point image (isolated within a single collicular hemifield) in Figure 4 using a nonlinear least squares regression (BU visual response in Figure 4A and C, $\sigma = 0.6 \pm 0.1$, $y_o = 0.007 \pm 0.002$, $x_o = 1.91 \pm 0.28$; TD preparatory response in Figure 4B and C, $\sigma = 1.33 \pm 0.13$, $y_o = -1.1 \times 10^{-6} \pm 4.8 \times 10^{-6}$, left SC: $x_o = -1.70 \pm 0.10$, right SC $x_o = 1.66$; saccadic motor response in Figure 4D, $\sigma = 0.54$, $x_o = 1.97$, $y_o = 0.003$). Errors denote standard deviations of the mean. In some cases, these independently calculated values were slightly different because of some small vertical and horizontal asymmetry (Figure 4A–D, top).

Two-dimensional Continuous Attractor Neural Field Model

We modeled the neural activity represented within the SCi temporally (relative to stimulus and saccadic events) and spatially (across the SC map) during saccade preparation and execution. We interpreted the input signals in the model to represent the physiological activity in the SCi that resulted from TD preparation signals and BU visual responses combining. We implemented a two-dimensional fully connected neural field model where the individual weights between connected nodes were dependent on their respective distances across the network and the instantaneous amount of activity within the network. We used a spatial interaction profile that exploited the local excitation and distal inhibition relationships measured within the retinotopic SC map (Dorris et al., 2007) that were described and modeled previously (Trappenberg et al., 2001).

External Inputs

Three different types of external inputs were used to represent the TD and BU signals that we recorded physiologically. The BU input signal reflected the responses produced by external visual stimuli. Two different kinds of TD inputs were used to reflect internally generated saccade-related signals that could occur across both SCi. One TD signal (Figure 5A, top) represented the spatial and temporal prediction signals in SCi BUNs that was present before the appearance of a saccade target stimulus (Figures 2D, 3B, and 4B) in the gap task (Dorris & Munoz, 1998; Dorris et al., 1997). Another TD signal (Figure 5A, bottom) represented an internally generated linear saccade decision signal similar to that proposed in the LATER model (linear accumulation to threshold with ergodic rate; Reddi & Carpenter, 2000; Carpenter & Williams, 1995) that influenced saccade selection based on the requirements of the task and the accumulated TD and BU information

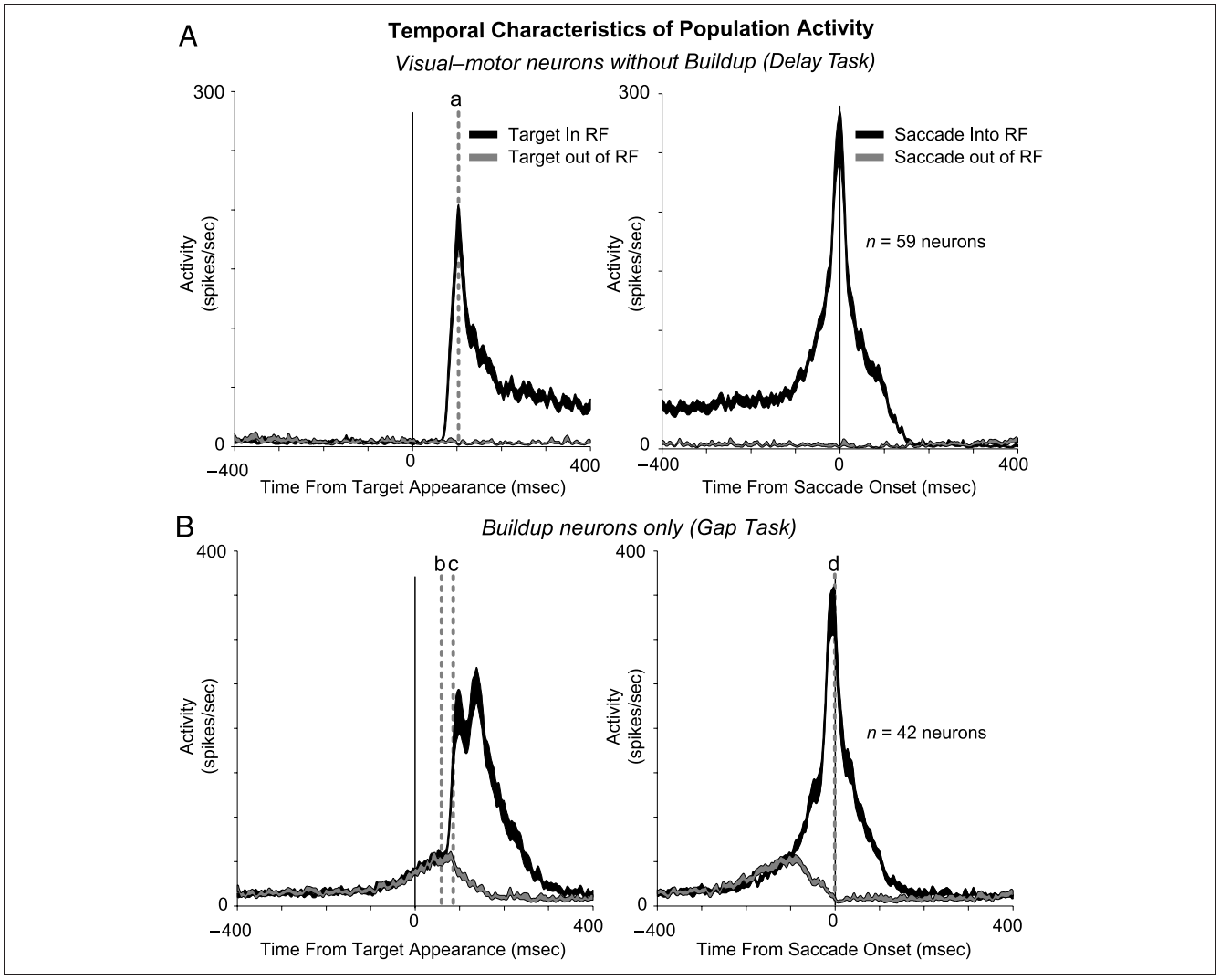

Figure 3. Population spike density functions of VMBNs in the delay task (A) and BUNs in the gap task (B) aligned on target appearance (left column) and saccade onset (right column). Dashed gray lines denote the times of the peak visual response in the delay task (Time a), preparatory buildup response in the gap task (Time b), combined visual and preparatory response in the gap task (Time c), and motor saccadic response in the gap task (Time c) that are plotted spatially on the SCi map and analyzed separately in Figure 5.

available (McPeek & Keller, 2002; Hanes & Schall, 1996; Schall, 1995). This signal differed from preparatory activity because it reflected the internally generated decision that the appropriate visual stimulus was present and should be foveated (Carpenter, 2004). The inclusion of this saccade decision signal was important to incorporate inputs from other visual or oculomotor brain regions that help to select the saccade target based on internally motivated task-related goals. This enabled the model to choose between multiple TD- or BU-driven saccadic goals and not always choose the strongest or most salient BU sensory input signal.

No central fixation signal was included in this model. Although the inclusion of a fixation signal is critical when modeling SRT differences between saccade tasks that utilize different levels of fixation engagement (as was demonstrated in Trappenberg et al., 2001, between overlap, step, and gap tasks as well as anti- and pro-saccade tasks), such a fixation signal was not required in the current model because the level of fixation engagement during the simulated saccade tasks was kept constant. Thus, it was not necessary to include a fixation signal to demonstrate the mechanism of how the spatial interactions of TD and BU signals in isolation can influence SRT. Furthermore, the addition of a fixation signal into the model only minimally increases global inhibition at each of the saccade locations, which results in a small but constant increase in SRT within all the simulated conditions.

Both the TD and BU external input signals were localized to the retinotopic positions of the simulated visual stimuli and saccade locations. The temporal dynamics of these external input signals were set to increase linearly to their maximum activation over a fixed interval. The BU visual and TD preparatory signals were defined to increase faster than the TD saccade decision signal. This made intuitive sense because the BU visual and TD preparation

signals are processed quickly once the target stimuli appeared, whereas the TD goal driven movement signal should be slower because it reflects a more cortically driven decision process (see Discussion). This balance ensured that lateral interactions between the BU and TD signals significantly impacted SRT, but the TD motor saccadic decision signal influenced which input signal would be selected for the saccade.

We imposed a linear increasing time course for the external TD preparatory and BU visual input signals:

$$I^{TD,BU}(t) = \begin{cases} \tilde{I}^{TD,BU}\left(\frac{t - t_{on}}{t_{on}^{TD,BU}}\right) & if\ t_{on} < t < t_{on}^{TD,BU} \\ \tilde{I}^{TD,BU} & else \end{cases} \quad (4)$$

wherein I is the maximum amplitude $\tilde{I}$ is a constant, t_{on} was the time of signal onset and $t_{on}^{TD,BU}$ was the time required for the buildup signal to saturate ($t_{on}^{TD,BU}$ = 173 msec). The TD saccadic decision signal that we employed was similar to that proposed in the linear LATER model (Carpenter, 2004; Reddi, Asrress, & Carpenter, 2003; Carpenter & Williams, 1995); however, in our implementation, it was a separate input signal that influenced the accumulation within the model and did not reflect the direct output of the model. Like the TD preparatory and BU visual signals, the TD saccadic decision signal increased linearly; however, it followed a slower rate of rise and was delayed relative to the pretarget TD preparation and BU visual response to ensure that there

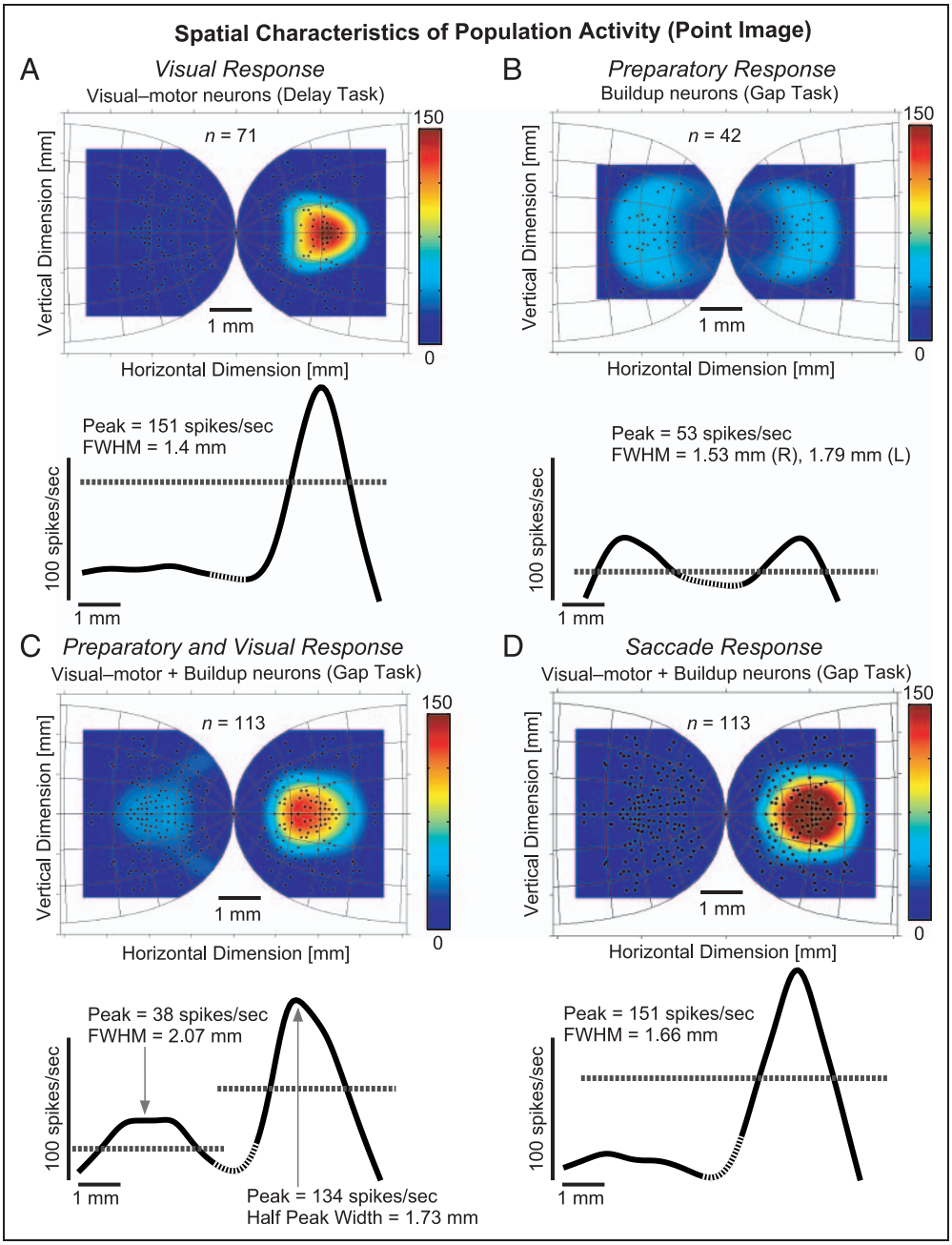

Figure 4. Spatial point images of BU visual, TD preparatory, and saccadic motor activity in the SCi map. (A) Top: Isolated visual response of VMBNs in the delay task for a 10° leftward target stimulus. Bottom: Cross-section of the visual response (above) from along the horizontal meridian. (B) Top: Isolated pretarget preparatory responses of BUNs in the gap task where the target could appear with equal probability 10° left or right of central fixation. Bottom: Cross-section of the preparatory responses (above) from along the horizontal meridian. (C) Top: Combined visual and preparatory response of combined BUNs and VMBNs in the gap task for a 10° leftward target stimulus immediately before the suppression of the preparatory activity at 10° right. Bottom: Cross-section of the visual and preparatory response (above) from along the horizontal meridian. (D) Top: Motor response of MBNs, VMBNs, and BUNs in the gap task for a 10° leftward saccade at movement onset. Bottom: Cross-section of the saccadic motor response (above) from along the horizontal meridian. (A–D) Dashed gray lines denote FWHM. Dashed black lines denote interpolated area of rostral SC where no neurons were recorded.

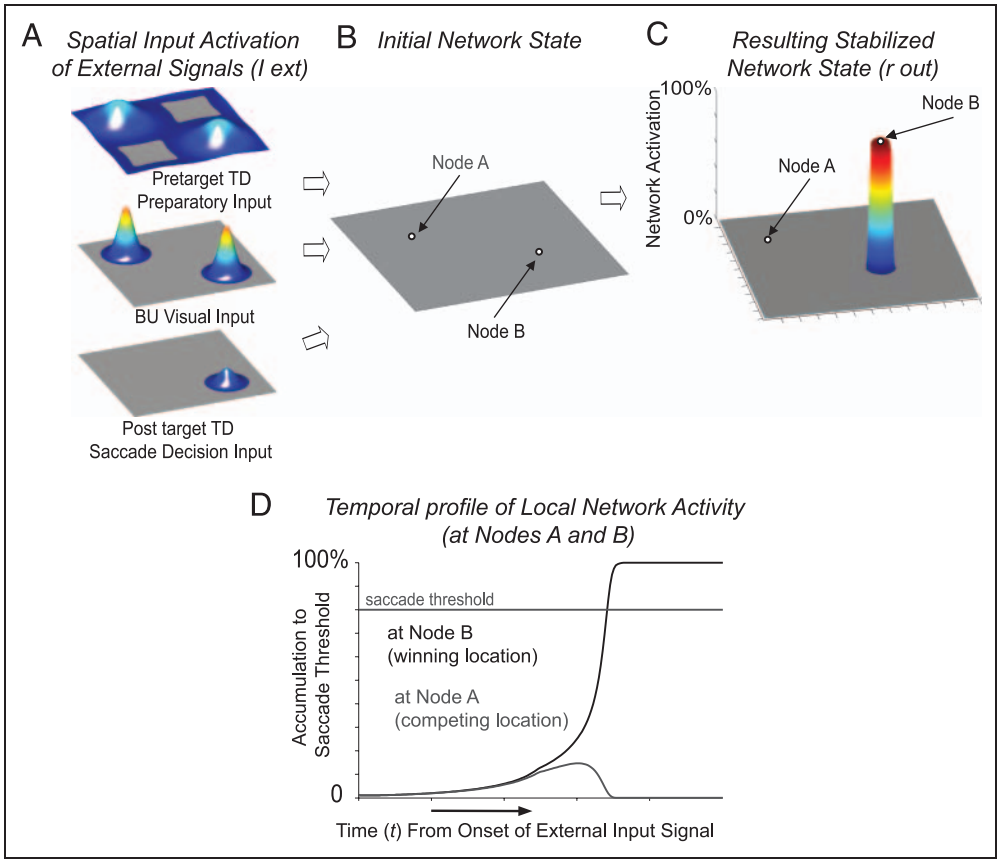

Figure 5. Implementation and functionality of the two-dimensional neurofield model. (A) Gaussian-shaped inputs (representing spatially defined TD and BU signals) are initially fed into the model. (B) The initial network state before onset of the TD and BU input signals. (C) Stable hill of activity maintained in the model after a dynamic winner-take-all competition has resolved the input signals. The accumulation of this activity resembles the rise to threshold of the saccadic motor command in BUNs that do not possess a visual response. (D) Activation of two neural nodes located at the direct center of the resulting saccadic motor command (Node A, black line) and competing location (Node B, gray line) in B and C (white circles).

was enough time for lateral interaction to occur between these other input signals. The TD saccadic decision signal was defined by

$$I_{Sac}^{TD}(t) = \begin{cases} 0 & if\ t_{on} < t < t_1 \\ \tilde{I}_{sac}^{TD}\left(\frac{t - t_{on}}{t_{sac}^{TD}}\right) & if\ t_1 < t < t_{sac}^{TD} \\ \tilde{I}_{sac}^{TD} & else \end{cases} \quad (5)$$

wherein $t_1 = 104$ msec and $t_{sac}^{TD} = 1041$ msec. Although the profile and magnitude of the local excitation remained constant, the magnitude of the lateral inhibition was dependent on the instantaneous amount of excitation within the model at any time. This insured that competing input signals were able to accumulate some activity within the model before the competing lateral inhibition shut them down. This assumption was based on recent physiological evidence in mouse SC showing local inhibitory circuitry within the SCi that followed a slower time course relative to local excitation (Phongphanee et al., 2008).

In Simulations 3 and 4, we increased the numbers of BU visual distractors (Simulation 3) or TD goal-related potential saccade locations (Simulation 4) from 1 to 2 to 4 to 6 to 8. In these simulations, each time the number of TD or BU signals was increased, the magnitude of the BU or TD signals was correspondingly decreased by 5%. This successive decrease incorporated the observed decrease in the visual response in the SC with increasing numbers of BU visual distractors (McPeek & Keller, 2002; Basso & Wurtz, 1998), as well as the decrease in TD preparatory activity with increasing numbers of potential saccade target locations (Basso & Wurtz, 1998).

Model Architecture

The interactions between TD and BU signals affected the time required by the model to accumulate to a single stable hill of activity (Figure 5C and D). Because the height of the TD and BU inputs were initially changing linearly over time, the total resulting input (I) at each node location at any time (t) is given by

$$I(t)^{in} = I(t)^{TD} + I(t)^{BU} \quad (6)$$

wherein all types of external TD or BU input have a Gaussian spatial shape such that the value of input at node location k is given by

$$\tilde{I}_k^{TD,BU} = a_{TD,BU}\, exp\left|\frac{((k - l)\Delta x)^2}{2\sigma_{in}^2}\right| \quad (7)$$

Here l is the location of the center of the input signal, Δx is the resolution of the model (2π divided by the number of neural nodes), and $a_{TD,BU}$ is either a constant (when constant magnitude of BU inputs are assumed)

or dependent on σ (when constant volume of BU inputs are assumed, Simulation 1 width manipulation only). The width of each of the TD inputs and BU inputs were derived from the corresponding point images on the SC (Figure 4).

The internal dynamics of the model in one dimension were described previously (Trappenberg et al., 2001). Here, we expanded the dynamic neural field $u(x)$ into two dimensions based on the following differential equation,

$$\tau \frac{\mathrm{d}u(\mathrm{x},t)}{\mathrm{d}t} = -u(x,t) + \int_0^{2\pi} \dots \int_0^{2\pi} w(|x-y|)\mathrm{A}(y,t)\ \mathrm{d}y_1 \dots \mathrm{d}y_2 + I^{in}(x,t) \quad (8)$$

wherein τ is a time constant and $w(|x-y|)$ is the weight kernel that defines the shape of spatial lateral interaction. The weight kernel is dependent on the distance between nodes and is parameterized by a negatively shifted Gaussian that results in identical local excitatory and distal inhibitory interactions at each node.

The activation A of the field is related to u by a sigmoidal gain function,

$$A(u) = \frac{1}{(1+e^{-\beta u})} \quad (9)$$

with a slope parameter β = 0.1. All node locations are scaled to values between 0 and 2π, and we consider a periodic field so that the neural map forms a torus.

The model implementation had 101 × 101 nodes that spanned two dimensions. This discrete form of the model is given by

$$\tau \frac{\mathrm{d}u_{i_x,i_y}(t)}{\mathrm{d}t} = -u_{i_x,i_y}(t) + \sum_{j_x} w_{i_x,i_y,j_x,j_y}\, A_{j_x,j_y}(t)\Delta x + I^{ext}_{i_x,i_y}(t) \quad (10)$$

wherein each node is indexed by i_x and i_y, respectively.

This grid is periodic such that nodes located at the edge wrap around their connections to the opposite side. A shift-invariant interaction profile was used because it was previously reported that visual and motor point images in the SC map were symmetrical and their size remained approximately constant and uniform across eccentricity (Marino et al., 2008). Accumulation to saccade threshold was plotted from the activity of the single neural node located at the center of the resulting dynamic winner-take-all activation (Figure 5D). This accumulation shared a comparable trend and similar temporal dynamics to the observed saccade-related signals in the SC (Figure 3B). Small differences in the temporal dynamics between network activity in the model (e.g., Figure 5D) and observed SC activity (Figure 3B) was permitted as long as the model predicted SRTs that closely matched experimentally observed ranges. The resulting network activation in the model represented the simulated activity of motor neurons in the SCi whose receptive field was likewise centered at the resulting saccade location (Marino et al., 2008).

Model Parameters

The time course necessary for the model to accumulate to saccade threshold determined the simulated SRT. Thus, all temporal parameters and time constants ($t_{on}^{TD,BU}$ and t_{sac}^{TD}) were set in order for the model to approximate the appropriate behavioral ranges of saccadic latencies reported in humans and monkeys (Marino & Munoz, 2009; Basso & Wurtz, 1998; Fischer, 1986; Boch, Fischer, & Ramsperger, 1984). Furthermore, the magnitude of TD and BU input signals in the model were likewise mapped to approximate equivalent signals in the frequencies of action potentials in VMBNs and BUNs in the SCi (Marino et al., 2008; Munoz & Wurtz, 1995a; Sparks & Hartwich-Young, 1989). We utilized a width of 0.5 mm as the standard deviation of the Gaussian shaped excitatory interaction profile to maintain accuracy and consistency with previous neurophysiological studies (Dorris et al., 2007; Munoz & Wurtz, 1995a). The maximal magnitude of distal inhibition was set to balance equally with the maximal magnitude of the local excitation to ensure that the parameter region of the model would resolve to a stable memory state that maintained the activity of the winner-take-all point image after all external inputs were removed (Kopecz, 1995; Kopecz & Schoner, 1995). We used an overall scale factor of 13 and an additional afferent delay of 50 msec to convert simulation cycle times to the rate of experimentally observed RTs.

Model Simulations

Multiple simulations were run utilizing BU and TD external inputs that were based on VMBN and BUN activities measured within the first 100 msec of visual target appearance (Figure 4). All simulations were set up and run from the theoretical time epoch when both BU and TD signals were simultaneously present within the SCi map (Figure 3B, Epoch b). In all simulations, the onset of spatially distinct external input signals (Figure 5A) resulted in winner-take-all behavior within the model. This winner-take-all mechanism resulted from competitive interactions between multiple external TD and BU signals within the network, which ultimately stabilized via lateral inhibitory interactions into a single Gaussian-shaped hill of activity that remained stable even after the external input signals were removed (Figure 5C; see Model Architecture above). The resolution of multiple signals in the network to a single hill of activity caused a nonlinear rise to threshold and

demonstrated the importance of spatial interactions within the SC (Figure 5D). Within each simulation, the external TD and BU signals increased linearly to their maximum activation and then were removed once network activity had stabilized.

The maintenance of a stable network activation after the removal of the external signals demonstrated that our model utilized a parameter region characterized by balanced excitation and inhibition that has been argued previously to be of particular interest for describing the saccadic systems (Kopecz, 1995; Kopecz & Schoner, 1995). After the onset of the TD and BU signals, the internal network dynamics resulted in a winner-take-all competition between each integrated external signal. Eventually, after several network iterations (discrete time steps (t) of the model as defined by Equation 10), a stable region (Gaussian-shaped hill) of activity out-competed all others and formed at the network location coding the chosen saccade vector. As this competition occurred, the Gaussian shaped field activation level at the winning location increased until a stable level was reached. We interpreted this activity increase at the winning location as a nonlinear accumulating saccade-related signal (Figure 5D). The accumulating saccade activity in the model most closely resembled the activity of BUNs that did not exhibit a visual response (MBNs). Once this signal crossed a fixed movement initiation threshold, the model was interpreted to trigger a saccade to that location. We chose an activation level of 80% (consistent with Trappenberg et al., 2001) of the peak of the final stable activity to represent the saccadic threshold trigger line as all other competing saccadic target locations were eliminated at this threshold level.

RESULTS

Spatial Properties of Visual, Preparatory, and Motor Point Images on the SC

We required neurophysiological data to constrain the model's parameters and ensure that it more accurately reflected the spatial patterns of activity in the primate SCi. Figure 4 illustrates point image population activity in the monkey SCi for a BU visual response (Figure 4A), a TD preparatory response (Figure 4B), a mixed BU and TD response (Figure 4C), and a saccadic motor response (Figure 4D). The peak of the BU visual response (Figure 4A) was calculated in the delay task (Epoch 2, Figure 2A) when the visual response was dissociated temporally from saccadic motor activity. In the spatially organized population of neurons we recorded, the peak visual response occurred 102 msec after target appearance and resulted in a visual point image with a peak of 151 spikes/sec. The width of each point image population response was calculated independently using two separate methods. First, to avoid any smoothing errors that could potentially have resulted from symmetrically mirroring activity above and below the horizontal meridian (see Methods), we calculated the activity occurring directly along the horizontal meridian (Figure 4A lower). From this activity profile along the horizontal meridian, we calculated the width of the activity at half of the peak. This width was 1.4 mm. Second, we also calculated the width from the full two-dimensional point image by fitting a two-dimensional Gaussian surface (Euler method) to the data and calculating the standard deviation (sigma). The sigma for the visual response in Figure 4A was $\sigma = 0.53$ mm (mean residual = -0.9).

We measured the peak of the TD pretarget preparatory activity during the gap task, in the epoch, immediately before the arrival of the target-aligned visual response (Epoch 6, Figure 2B), which is when the peak preparatory activity occurred (Figures 2D and 3B). The maximal preparatory response occurred 55 msec after target appearance and resulted in two point images, one on each side of the SC that were centered at the location of the two equally probable potential target locations (10° left or right, Figure 4B). The maximum value of the TD preparatory activity was 53 spikes/sec. The mean FWHM calculated along the horizontal meridian was 1.53 mm (right) and 1.79 mm (left; Figure 4B, bottom). The Gaussian fitted sigma for these two TD responses were $\sigma = 1.35$ mm (mean residual = -0.97; right) and $\sigma = 1.45$ mm (mean residual = -1.05; left).

In the gap task, we recorded a brief period when both BU visual and TD preparatory responses were present within the right SCi and an isolated TD preparatory response was simultaneously present in the left SCi (Figures 3B and 4C). This temporal overlap occurred because at the time of the earliest part of the visual response the preparatory activity in the opposite SC had not yet been eliminated. Thus, although the TD preparatory spatial prediction signal (opposite to the target) preceded the onset of the BU visual response, it persisted long enough to compete and/or interact with it. The existence of this physiological epoch is critically important for our model simulations because it justifies the simultaneous input of TD and BU signals into the model to study how their competitive spatial interactions influenced SRT. Within the population of neurons recorded, the maximum combined BU and TD responses occurred in the gap task 90 msec after target appearance. This resulted in two point images, one on each side of the SC that were centered at the location of the target (Figure 4C, right SC) and the equally likely potential location where the target could have, but did not, appear (Figure 4C, left SC). Here, the peak of the BU visual activity was 134 spikes/sec and the peak of the TD preparatory activity was 38 spikes/sec. The peak TD preparatory activity illustrated in Figure 4C was reduced relative to Figure 4B because this combined BU and TD population point image included VMBNs that did not exhibit TD preparatory activity. The mean FWHM calculated along the horizontal meridian (Figure 4C, bottom) was 1.73 mm for the BU visual response and 2.07 mm for the TD preparatory response. The Gaussian fitted sigma for these were $\sigma = 0.67$ mm (mean residual = -0.12, right

BU visual) and σ = 1.19 mm (mean residual = −0.35, left TD preparatory).

Finally, we also measured the height and width of the peak of the saccadic motor burst from saccade-aligned activity in the gap task (Figure 4D). The peak of this saccadic motor burst was 218 spikes/sec. The FWHM calculated along the horizontal meridian (Figure 4D, bottom) was 1.66 mm. The Gaussian fitted width was σ = 0.54 mm (mean residual = 1.7).

Simulation 1: Spatial Interactions within Single Input Signals

Recent evidence has shown that the magnitude of visual responses of individual SC neurons are modulated by stimulus properties such as contrast (Li & Basso, 2008) and luminance (Marino et al., in revision). This suggests that the corresponding magnitude of these visual response point images were also changing. It is not known, however, whether the width of the point images on the SC map was also affected by luminance or contrast. SRTs have been shown to decrease to a minimum with increasing target luminance (Jaskowski & Sobieralska, 2004; Doma & Hallett, 1988; Boch et al., 1984) or contrast (White, Kerzel, & Gegenfurtner, 2006; Carpenter, 2004; Ludwig, Gilchrist, & McSorley, 2004). However, our recent study (Marino & Munoz, 2009) suggested that SRT initially decreased with increasing target luminance but then increased again at brighter luminance levels. Here we assess how changes to the height (magnitude) or width of point images (Figure 1B) in the model can explain these previous results.

Effects of Input Signal Magnitude

To assess the effect of input signal magnitude on saccadic latency in the model, we varied the peak magnitude of the input signal across seven different values that ranged from 65 to 375 spikes/sec (Figure 6B) while keeping the width of the signal constant at σ = 0.6 mm. These ranges were used to approximate the BU visual responses that were reported within SCi neurons when luminance or contrast was manipulated (i.e., from below 50 spikes/sec to more than 350 spikes/sec; Marino et al., in revision; Li & Basso, 2008). When the magnitude of the input was increased (Figure 6A–C), the time required by the model to reach saccadic threshold (simulated SRT) decreased (Figure 6C) in a manner similar to previous behavioral results (White et al., 2006; Carpenter, 2004; Jaskowski & Sobieralska, 2004; Ludwig et al., 2004; Doma & Hallett, 1988; Boch et al., 1984). At low magnitude (65 spikes/sec), simulated SRT was 383 msec, whereas at high magnitude (375 spikes/sec), simulated SRT decreased to 133 msec.

Effects of Input Signal Width

To date, no study has examined whether altered stimulus properties can affect the size of BU visual point images in the SC; therefore, we examined how input signal size influenced SRT in our model (Figure 1B). This is an important simulation because we hypothesized that increases in activation area could cause decreases or increases in SRT, depending on the area of the SC map activated. This possible relationship between the size of SCi point images and SRT could explain our previous finding that SRT can decrease or increase with increasing luminance (Marino & Munoz, 2009).

To assess the effect of signal width on saccade latency independently, we manipulated the width of the Gaussian shaped input while keeping the peak magnitude constant (150 spikes/sec, a physiological range that matched the peak of our isolated visual response point image in Figure 4A). We systematically altered the width (σ) of the input from 0.4 to 2.1 mm (Figure 6D–F) to insure that we did not exceed the upper or lower width range of our recorded BU or TD point images by more than 70% (see Figure 4). We did not alter the width beyond these values because larger or smaller values would probably be too far removed from realistic physiological ranges in the SCi (range, from 0.54 mm for the motor burst to 1.45 mm for the preparatory buildup). When the width was increased from 0.4 to 2.1 mm, simulated SRT decreased from 230 msec (σ = 0.4 mm) to 189 msec (σ = 1.2 mm) and then increased again up to 200 msec (σ = 2.1 mm, black line in Figure 6E and F). This resulted in a U-shaped SRT function when width was increased and the magnitude of the input signal was kept constant. The initial decrease in SRT that we observed resulted from increases in the width dependant volume of the input signal. However, as the width of the signal increased beyond the excitatory width of the interaction profile within our model (Figure 1B, right), the surrounding inhibition became activated and caused an 11-msec increase in SRT when the width was increased from 1.2 to 2.1 mm. When the external inhibition was increased by 20% (achieved by globally shifting the interaction profile more negatively, see Methods), the SRT increase with increasing signal width was 30 msec (difference from 1.2 to 2.2 mm within dotted line only). Although this relationship follows our initial prediction, the increase in SRT did not occur for all signals that were wider than the excitatory interaction profile. In our model, we only observed this increase in SRT when the input width was between 240% and 278% above that of the excitatory interaction profile. By changing the width (while keeping the magnitude of the signal constant), we made the assumption that the overall volume of the signals were changing.

Constant Volume Hypothesis

It is possible that the magnitude of point images does not remain constant but that the volume of the overall activity (regardless of its width or magnitude) might remain constant across different conditions. If this is the case, a constant volume of neural activity would require

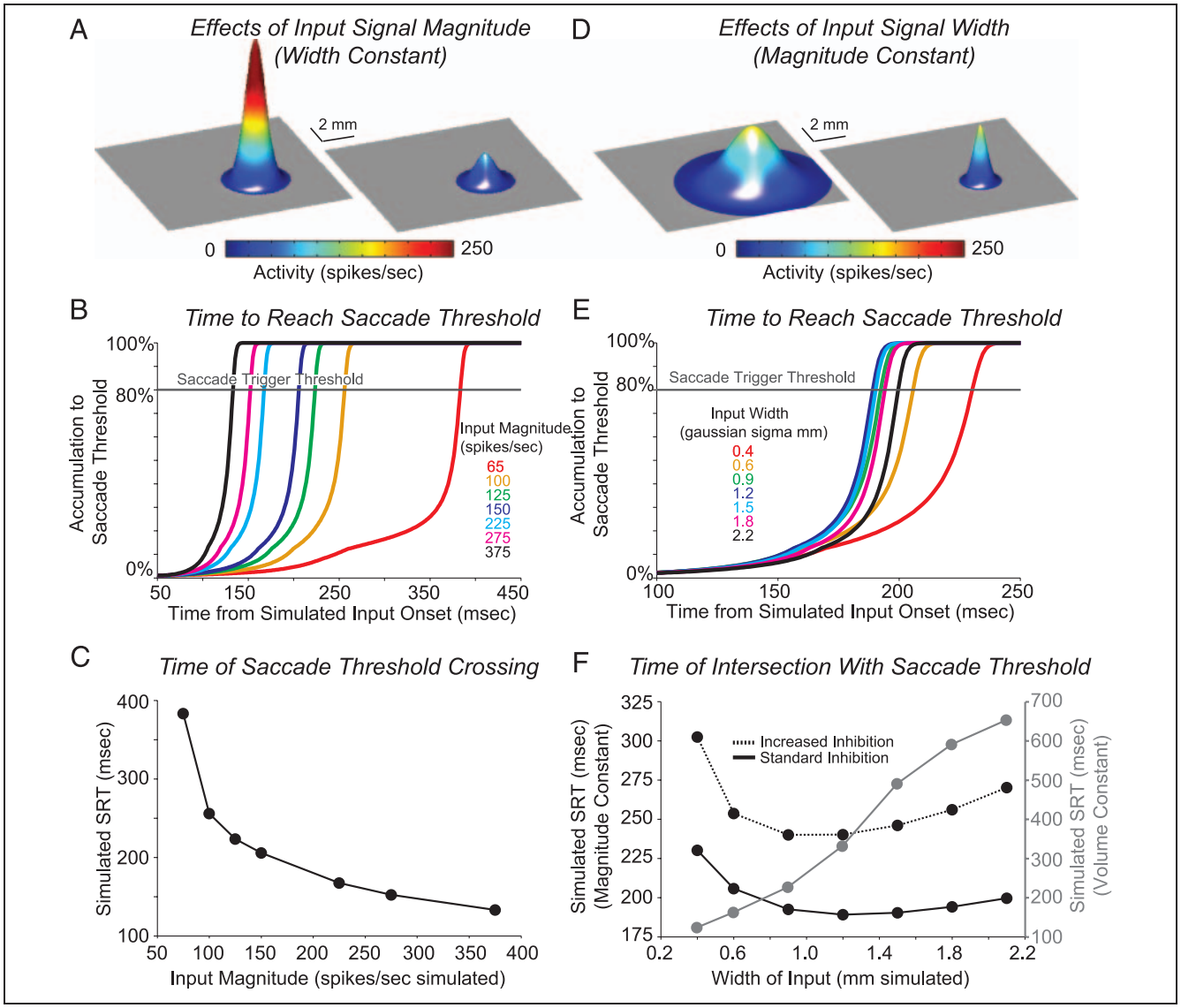

Figure 6. Simulations of the effects of magnitude (A–C) and width (D–F) of a single input signal on modeled SRT. (A and D) Examples of strong (375 spikes/sec; A, left) and weak (65 spikes/sec; A, right) input signal magnitudes and wide (σ = 1.5 mm; D, left) and narrow (σ = 0.4 mm spikes/sec; D, right) input signal widths modeled. (B and E) Accumulation to saccade threshold of a neural node centered at the spatial dynamic winner-take-all network location coding the resulting saccade over a range of signal input magnitudes (B) and widths (E). (C and F) Modeled SRT for each input signal magnitude (C) and width (F) tested based on saccadic threshold crossing time. Solid and dotted black lines denote effects of signal width (with constant magnitude) on SRT (F). Dotted black line denotes the effect of increasing global inhibition relative to the solid black line. Gray data points in F denote effects of changing width while keeping volume of activation constant (i.e., signal magnitude decreases with increasing width to maintain constant volume).

normalization between the width and the peak. Thus any increase in signal width would result in a corresponding decrease in its peak magnitude to ensure that the overall activity (volume) integrated over the SCi map remained constant.

To examine this constant volume assumption, we manipulated signal width without the assumption of constant magnitude. In these simulations SRT increased approximately linearly with increasing signal width from 124 msec (σ = 0.4 mm) to 653 msec (σ = 2.1 mm; Figure 6F solid gray line). Because the constant volume condition resulted in decreases in peak magnitude with each increase in signal width, the observed increases in SRT were most strongly influenced by these corresponding decreases in peak magnitude.

Simulation 1 Summary

Our model predicted that any changes to the magnitude or the width of point images within the SCi map should influence SRT. As the magnitude of the input signal was increased, SRT decreased. As the width of the input signal was increased, SRT either increased or decreased then increased, respectively depending on whether a constant magnitude or constant volume signal was used. On the basis of these results, the decrease of SRT with

increasing target luminance (Bell, Meredith, Van Opstal, & Munoz, 2006; Jaskowski & Sobieralska, 2004; Doma & Hallett, 1988; Boch et al., 1984) or contrast (White et al., 2006; Carpenter, 2004; Ludwig et al., 2004) previously reported likely results from increases to the magnitude (Marino et al., in revision; Li & Basso, 2008) of the peak visual response in the SC. The model also predicted that changes to the spatial width of input signals also affected SRT such that increasing the spatial width decreased SRT until it was wide enough to extend beyond the region of local excitation and into inhibitory regions of the map (Figure 1B). The decreases followed by increases in SRT with increasing luminance that we previously reported (Marino & Munoz, 2009) could be explained by increases to the width of visual point images in the SCi.

Simulation 2: Effects of Spatial Signal Distance

It has been reported previously that saccades to two targets elicit a greater proportion of short latency express saccades when the targets are closer together (i.e., located within 45° of each other; Edelman & Keller, 1998). This result suggests that SRT can be reduced when competing point images are close enough together to overlap. In our model, the distance between point images similarly determines if they will overlap and summate or compete over a larger distance. We examined how the spatial distance between TD- or BU-related saccade signals in the model interacted to influence SRT. Figure 7 shows how SRT was influenced by the spatial distance between two distinct input signals of equal size. When the magnitude of the input signals matched the magnitude of the isolated visual response point image (150 spikes/sec, $\sigma = 0.6$ mm; Figure 4A), SRT increased with increasing distance between the nodes up to 1.2–2.4 mm (Figure 7B and C). Further increases in distance had no effect on SRT. To determine whether this effect of distance was dependant on the strength or magnitude of the two competing signals, we also examined weak magnitude (65 spikes/sec, which approximated the lower frequency TD preparatory signals that we recorded) and strong magnitude (375 spikes/sec, which approximate the highest frequency discharge of visuomotor burst neurons that we recorded of which 23% had a peak visual response above 350 spikes/sec in the delay task) signals independently. As the magnitude of the two competing signals decreased, the influence of distance between the signals increased in the simulations (Figure 7B and C). Specifically, at an input magnitude of 65 spikes/sec, the increase in SRT between pairs of signals located 0.5 mm apart and 2.4 mm apart was 162 msec (0.5 mm: 237 msec, 2.4 mm: 399 msec; Figure 7C, light gray circles). At an input magnitude of 375 spikes/sec, the increase in SRT between pairs of signals located 0.5 mm apart and 2.4 mm apart was only 41 msec (0.5 mm: 109 msec, 2.4 mm: 150 msec; Figure 7C, light black circles).

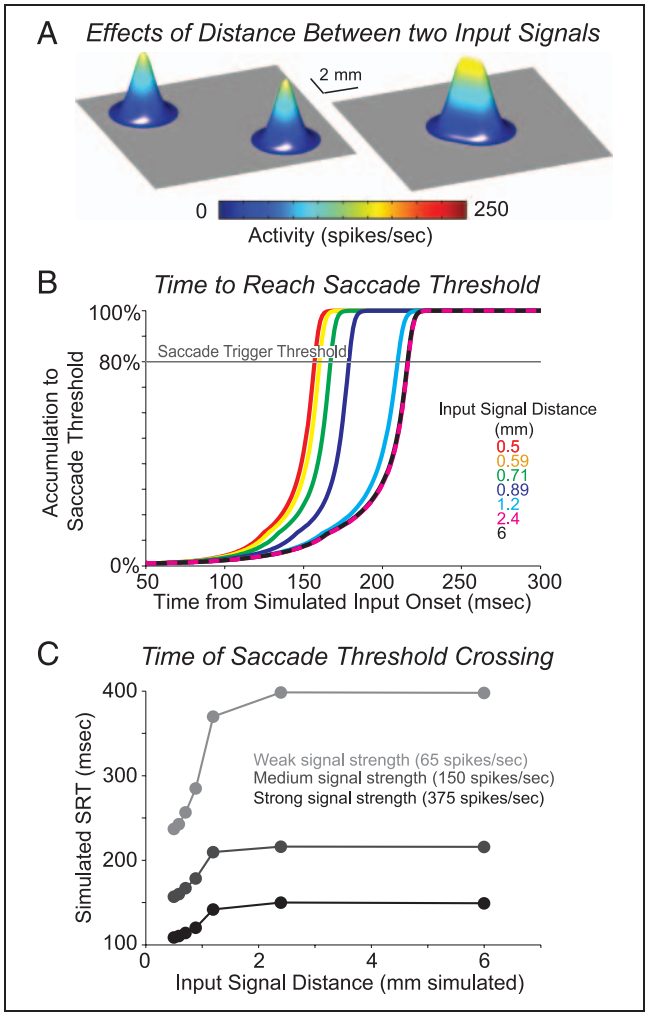

Figure 7. Simulations of the effects of distance between two single input signals on modeled SRT. (A) Examples of distant (6 mm, left) and nearby (0.89 mm, right) input signal distances. (B) Accumulation to saccade threshold of a neural node centered at the spatial dynamic winner-take-all network location coding the resulting saccade over a range of signal input distances. (C) Modeled SRT for each input signal distance (weak magnitude: black line, 65 spikes/sec; medium magnitude: dark gray line, 150 spikes/sec; and strong magnitude: light gray line, 375 spikes/sec) tested based on saccadic threshold crossing time.

Simulation 2 Summary

The model predicted that overlapping point images (both TD and BU) reduced SRT compared with nonoverlapping point images because overlapping point images summated to reduce the time to accumulate to saccade threshold (Figure 1C). Therefore the distance between visual stimuli or potential saccade target locations in the visual field significantly influenced SRT. Furthermore, the influence of spatial distance between input signals on SRT was strongest for weaker signals, as these require more time to accumulate to saccade threshold and were thus more susceptible to be influenced by such spatial interactions. This result supports a previous study (Edelman & Keller, 1998) that showed increases in short latency saccades when multiple

target stimuli were presented within the same 45° arc of visual angle (the approximate angular width of a BU visual point image in the SC; Marino et al., 2008; Anderson et al., 1998).

Simulation 3: The Effects of the Number of Competing BU Signals

During visual search experiments, a target must compete with distractor stimuli that are simultaneously present on the retina and compete for foveation by the saccadic system (Schall & Thompson, 1999). Previous studies of visual search have demonstrated that the addition of distractors increases SRT compared with when only one target stimulus is present (Arai, McPeek, & Keller, 2004; McPeek & Keller, 2001; McPeek & Schiller, 1994). Further increasing the number of distractors, however, has been shown to both increase and decrease SRT. Increases in SRT with increasing distractors ("set-size effect") has been suggested to result from increases in the time needed to find a target among increasing numbers of distractors (Cohen, Heitz, Woodman, & Schall, 2009; Balan, Oristaglio, Schneider, & Gottlieb, 2008; Shen & Pare, 2006; Carrasco & Yeshurun, 1998). However, other visual search experiments have instead shown that increasing numbers of distractors can also decrease SRT without sacrificing accuracy (Arai et al., 2004; McPeek, Maljkovic, & Nakayama, 1999). This reverse of the "set-size effect" has been hypothesized to be related to a BU grouping process that shifts attention to the target more quickly when distractor densities are greater (Bravo & Nakayama, 1992).

To determine whether these differing effects of distractor number on SRT could be explained by spatial competition within our model, we examined the effects of 1, 2, 4, 6, or 8 competing BU signals. We utilized magnitude and width profiles for the target and distractor stimuli that matched those of the isolated visual response point image in the SCi that we recorded in the delay task to maximize physiological accuracy (Figures 2A and 4A). In the simulations, the BU signals were placed at equally spaced locations around a circle that was centered at the midpoint of the model. This midpoint represented the center of the foveal region in the SCi, located between the rostral poles of each colliculus (Krauzlis, 2003; Munoz & Wurtz, 1993). Even numbers of signals were mirrored across the vertical meridian to ensure symmetry and equal weighting between the left and right SC (Figure 8A and D). Because the simple distance between input signals alone was shown to affect our simulated SRTs significantly (Figure 7), we examined the effects of multiple BU signals at two independent distances across the left and right SC: far (6 mm diameter circle) and near (0.67 mm diameter). The far distance ensured that each BU signal remained spatially distinct when up to eight signals were simultaneously presented (Figure 8A). The near distance ensured that the multiple BU signals would be close enough together to have overlapping point images of activity that would interact via summation (Figure 8D). The gray line and data points in Figure 8E and F denote simulations where the magnitude of the BU signals did not decrease with increasing numbers of signals (see Methods).

When distant BU inputs were used, simulated SRT increased linearly with increasing numbers of competing targets from 1 (206 msec black and gray lines) to 8 (295 msec black, 261 msec gray; Figure 8B and C). In contrast, when near BU inputs were used (Figure 8E,F), simulated SRT increased linearly with increasing numbers of competing targets from 1 (206 msec black and gray lines) to 2 (221 msec black, 216 msec gray) to 4 (240 msec black, 230 msec gray) targets, but then decreased from 4 to 6 (230 msec black, 224 msec gray) to 8 (216 msec black, 207 msec gray) targets. The initial increase in SRT up to four signals, resulted from increased competition from relatively few targets; however, when sufficiently large numbers of BU signals were present, the activity from each signal summated together to increase network excitability over a larger area of the model, and this resulted in an overall reduction of SRT. The trend was the same when the magnitude of the BU signals did not decrease with increasing numbers of signals; however, the overall magnitude of the effect was slightly decreased.

Simulation 3 Summary

The model predicted that increasing the number of visual stimuli increased SRT when the corresponding point images in the SC were spatially separate, but decreased SRT when the point images overlapped (Figure 1C). This suggests that different set-size effects can result, depending upon the distance between the point images of the target and multiple visual distractors. This simple result can explain the apparent discrepancies between classical set-size effects (where SRT increases with increasing numbers of distractors; Cohen et al., 2009; Balan et al., 2008; Carrasco & Yeshurun, 1998) and other studies which show decreases in SRT (with corresponding increases in saccade accuracy) with increasing numbers of visual distractors (Arai et al., 2004; McPeek et al., 1999).

Simulation 4: Effects of Number of Competing TD Signals

In addition to the competition that can occur between multiple BU stimuli, multiple TD signals can also be present in the SCi simultaneously (when foreknowledge of task related goals exists) to influence SRT (Story & Carpenter, 2009; Basso & Wurtz, 1998; Dorris & Munoz, 1998; Figure 4B and C). The effects of TD spatial target probability on SRT have been studied previously, and many seemingly contradictory results have been reported. Specifically, decreasing spatial target predictability has been shown to influence SRT in many different ways including no change (Kveraga & Hughes, 2005; Kveraga, Boucher, & Hughes, 2002), increases (Story & Carpenter, 2009; Basso & Wurtz,

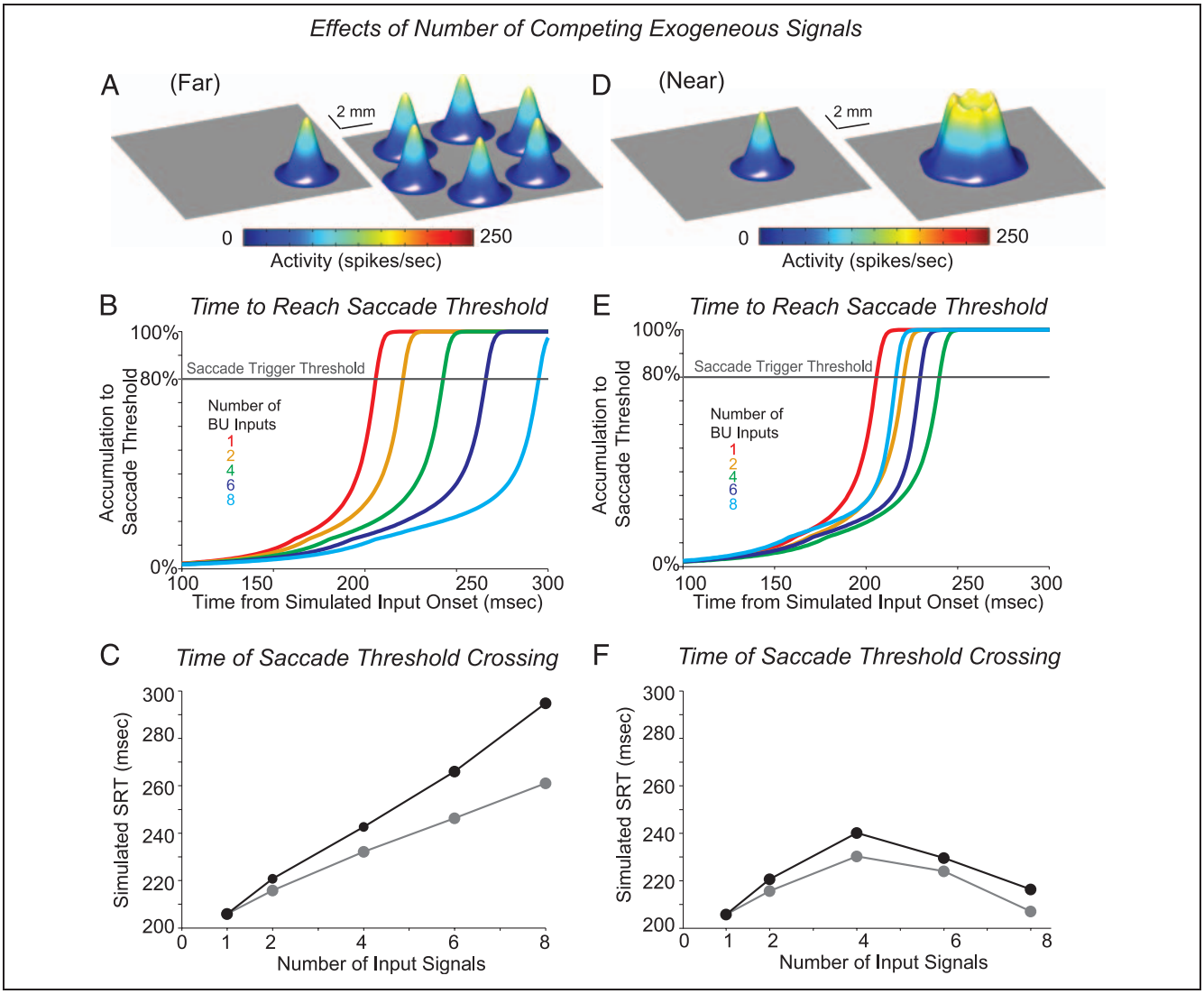

Figure 8. Simulations of the effects of number of competing BU inputs both nearby (A–C) and far (D–F) from central fixation on modeled SRT. (A and D) Examples of individual (left) and multiple (six inputs, right) BU input signals at distant (3 mm from central fixation; A, left) and nearby (1 mm from central fixation; D, right) locations within the network. (B and E) Accumulation to saccade threshold of a neural node centered at the spatial dynamic winner-take-all network location coding the resulting saccade over a range of signal numbers for distant (B) and nearby (E) signals. (C and F) Modeled SRT for each number of input signals for distant (C) and nearby (F) targets. Gray lines and data points denote identical simulations where the magnitude of the BU inputs did not decrease with increasing numbers of signals (see Methods).

1998), decreases (Lawrence, St John, Abrams, & Snyder, 2008), and U-shaped increases and then decreases (Marino & Munoz, 2009). Although these results appear to be in conflict, we show how each of them can be reproduced by altering the spatial properties of the underlying TD and BU signals (size, magnitude, distance apart, and number of signals).

Figure 4C demonstrated that both BU and TD signals were present in the SCi map simultaneously, and we recreated this epoch to explore how the spatial competition between these different signals influenced SRT. We set up simulations with 1, 2, 4, 6, or 8 TD input signals and set the magnitude and width of these signals to match the corresponding point images that we recorded in the SCi (Figure 4B and C). In addition to the TD signals, we also included one BU signal (with width matched to the visual response point image Figure 4C) to mimic the single resulting visual input generated by target appearance. We increased the magnitude of the TD signal to 65 spikes/sec (which was larger than the population average but still within the overall physiological range of this population) in order for it to be large enough to significantly influence the network activity in the model. All simulations were tested independently at two distances: far (6 mm diameter circle) and near (0.67 mm diameter circle). The far distance (6 mm diameter) ensured that BU and TD signals were spatially distinct when up to 8 were simultaneously presented (Figures 1C, left, and 9A) and the near distance (0.67 mm) ensured that these signals were close enough together to have overlapping activity (Figures 1C, right, and 9D). The gray line and data points in Figure 9E and

F denote simulations where the magnitude of the TD signals did not decrease with increasing numbers of signals (see Methods).

Results were generally similar to Simulation 3. When distant TD inputs were used, simulated SRT increased approximately linearly with increasing numbers of competing TD signals from 1 (209 msec, black and gray lines) to 8 (237 msec, black; 245 msec, gray; Figure 9A–C). However, when nearby TD inputs were used, simulated SRT decreased approximately linearly with increasing numbers of competing targets from 1 (209 msec, black and gray lines) to 8 (147 msec, black; 136 msec, gray; Figure 9D–F). Because the TD signals were wider than the BU signals (σ = 0.6 mm vs. σ = 1.42 mm; see Figure 4), their activity summated together with as few as two signals to more easily increase network excitability over a larger area and thereby reduce SRT. The trend was the same when the magnitude of the TD signals did not decrease with increasing numbers of signals; however, the overall magnitude of the effect was differed slightly.

Simulation 4 Summary

The model predicted that increasing the number of TD pretarget signals could increase or decrease SRT depending on the amount of overlap of their point images in the SCi map. Specifically, when the number of nearby TD potential target locations increased, the corresponding point images overlapped leading to reduced SRT via excitatory summation. In contrast, when the number of distant TD potential target locations increased, the corresponding point images remained separate, leading to increased

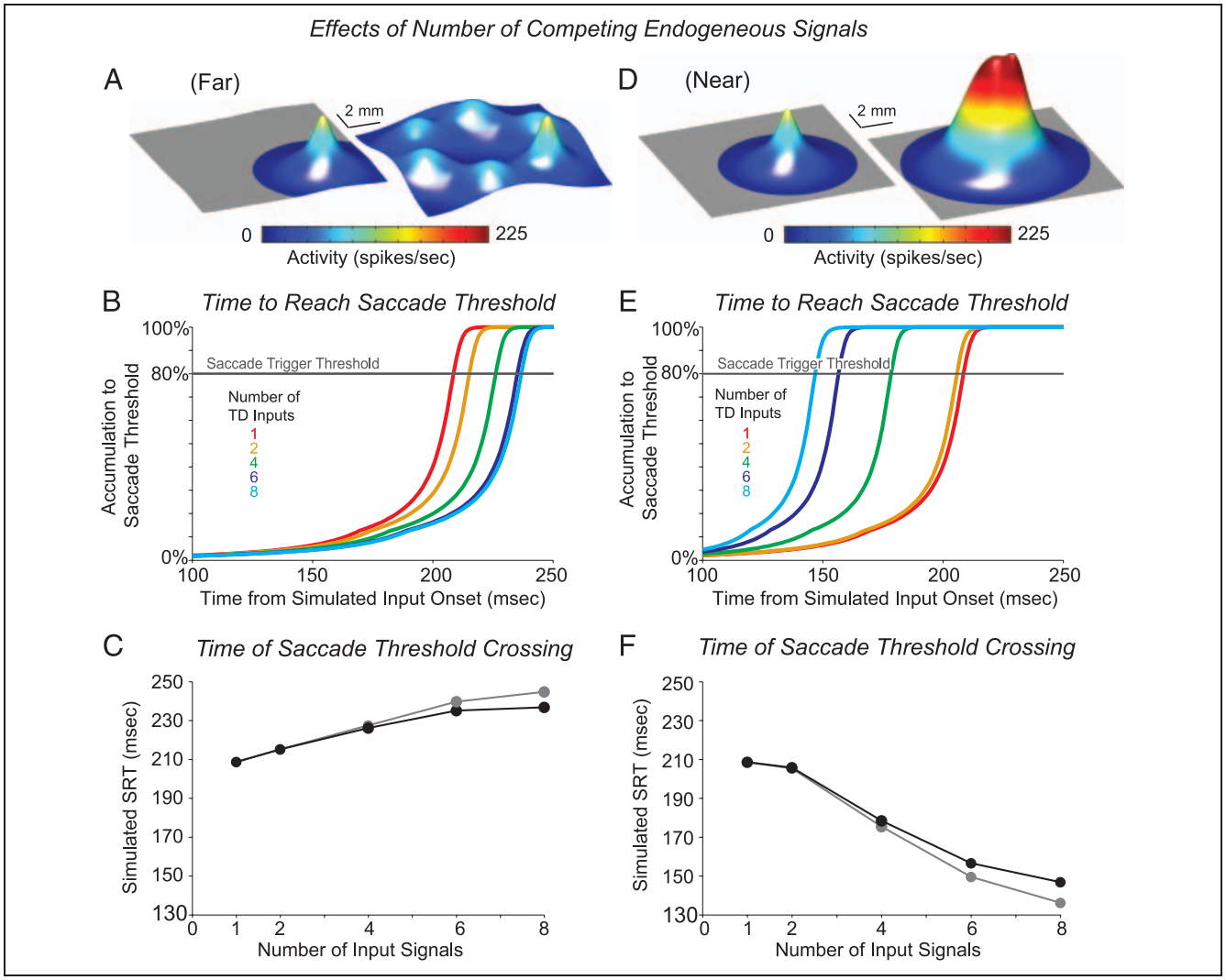

Figure 9. Simulations of the effects of number of competing TD inputs on modeled SRT for signals located nearby (A–C) and far (D–F) from central fixation (1 BU signal representing the appearance of the visual target was always presented at the resulting saccade location). (A and D) Examples of individual (left) and multiple (six inputs, right) BU input signals at distant (3 mm from central fixation; A, left) and nearby (1 mm from central fixation; D, right) locations within the network. (B and E) Accumulation to saccade threshold of a neural node centered at the spatial dynamic winner-take-all network location coding the resulting saccade over a range of signal numbers for distant (B) and nearby (E) TD signals. (C and F) Modeled SRT for each number of TD input signals for distant (C) and nearby (F) targets. Gray lines and data points denote identical simulations where the magnitude of the TD inputs did not decrease with increasing numbers of signals (see Methods).

SRT via lateral inhibitory competition (Figure 1C). It is possible that this mechanism could explain the complex results of previous studies that have shown no change (Kveraga & Hughes, 2005; Kveraga et al., 2002), increases (Story & Carpenter, 2009; Basso & Wurtz, 1998), decreases (Lawrence et al., 2008), or increases followed by decreases in SRT (Marino & Munoz, 2009) with increasing numbers of potential saccade target locations. Each of these different results potentially could be explained by this model via different combinations of spatially interacting point images (i.e., magnitude, width, and the relative amount of overlap). For example, Kveraga et al.'s (2002) observations that showed no change in SRT with increasing potential target locations could result from some combination of spatial parameters where the increase in SRT caused by increasing potential target locations (Figure 9C) was balanced by the decrease in SRT caused by increasing their overlap (Figure 9F). Likewise, for a different combination of parameters, Marino and Munoz's (2009) U-shaped result could be explained if increasing potential target locations are initially spread out enough to increase SRT (Figure 9C) until their increased overlap (caused by increasing numbers of potential targets) then causes SRT to decrease (Figure 9D).

DISCUSSION

Here, we presented a new two-dimensional neural field model of the SCi to account for many previous complex and contradictory results regarding how BU or TD signals converge to influence SRT via the spatial interactions of their point images. We demonstrated that the spatial properties (magnitude, width, distance apart, or number of competing signals) of the underlying TD or BU signals on the SCi map influenced SRT. We presented new neurophysiological data, recorded from neurons in the SCi that were used to calculate point image size and constrain the model parameters. These physiological point images represented isolated BU visual responses, TD preparatory activity, and saccadic motor bursts that were spatially organized within the SCi map. BU visual point images had greater magnitude and a narrower width relative to TD preparatory point images. During the initial part of a BU visual response to an appearing saccade target stimulus, TD preparatory activity persisted briefly (at other expected target locations) elsewhere within the SCi map. This suggests that winner-take-all competition between separate TD and BU signals takes place within the SCi map. Our model demonstrates how during this period of overlap, TD and BU signals compete to determine where the next saccade will be directed. The model made novel and experimentally supported predictions about the properties and spatial interactions of TD and BU signals in the SCi.

The model demonstrated several simple principles that govern how spatial signals (BU or TD) interact within the SCi map to influence SRT: For individual input signals (BU or TD), increasing the peak magnitude of an input decreased SRT while increasing the width decreased SRT until it spread beyond local excitatory distances into inhibitory ranges, which then caused SRT to increase (Figure 1A and B). Increasing the number of spatially separate input signals (TD or BU) increased SRT when the point images were spatially distant in the map and decreased SRT when these point images were close enough to overlap and summate (Figure 1C). Thus, the model demonstrates how the spatial interactions of individual or multiple TD and BU point images can influence visually guided saccade behavior.

An Expansion of Linear Saccade Accumulator Models

Linear accumulator models remain a popular and useful framework for describing the neural processes underlying saccade initiation. One such model (LATER) assumes that a saccadic decision signal increases linearly until a neural threshold is crossed and a saccade is triggered to a specific location (Carpenter, 2004; Munoz & Schall, 2003; Hanes & Schall, 1996; Carpenter & Williams, 1995). Neural correlates of this accumulation signal have been identified within neurons located within both the FEF (Everling & Munoz, 2000; Hanes & Schall, 1996) and the SCi (Paré & Hanes, 2003; Dorris & Munoz, 1998; Dorris et al., 1997). Previously, this model has been used successfully to describe a simplified neural framework that can explain a wide range of SRT variations including speed versus accuracy trade-offs (Reddi & Carpenter, 2000), contrast and probability (Carpenter, 2004), task switching (Sinha, Brown, & Carpenter, 2006), reading (Carpenter & McDonald, 2007), and the gap effect (Story & Carpenter, 2009). However, the limitations of LATER are evident whenever the effects of TD or BU experimental manipulations on SRT are nonlinearly related, such as the complex increases and decreases in SRT we have explained here via lateral interactions. In the current study, we used linear input signals to represent each individual TD and BU signal within the model. In particular, a TD saccade decision signal was required by the model to reinforce the specific BU sensory or TD task-related signal that represented the appropriate saccade target goal. This ensured that the correct visual stimulus was chosen over the visual distractors or other potential target locations. This TD saccadic decision signal is conceptually very similar to the decision signal described by the LATER model. By incorporating a linear accumulating decision signal within our neural field, we utilized an underlying neural mechanism that was conceptually similar to LATER; however, we extended its predictive power into the nonlinear domain. This enabled our model to be robust enough to explain the nonlinear and apparently contradictory behavioral results from previous studies of TD and BU influences on SRT. This additional explanatory and predictive power was achieved

via the spatial interactions of competing point images that resulted from the lateral interactions that are hypothesized to be present within the SCi map (Dorris et al., 2007; Munoz & Fecteau, 2002; Munoz & Istvan, 1998).

Oculomotor Violations of Sensorimotor Transformation Laws

Simple laws govern the basic effects of BU and TD processes on motor response latencies across sensory modalities. Hick's law states that response latencies increase as a log function of the number of possible choice response alternatives (Hick, 1952). Here, we have modeled several seemingly contradictory studies that have shown agreement with (Thiem, Hill, Lee, & Keller, 2008; Lee, Keller, & Heinen, 2005; Basso & Wurtz, 1998) and violations of (Marino & Munoz, 2009; Lawrence et al., 2008; Kveraga & Hughes, 2005; Kveraga et al., 2002) Hick's law. Our simulations have demonstrated that the degree of overlap between potential saccade target locations within the SCi map can lead to both agreement with (separate point images compete and increase SRT) and violations of (overlapping point images summate and reduce SRT) Hick's law in the oculomotor system.

Pieron's law mathametically describes a hyperbolic decay function between stimulus intensity and response latency, such that RT logarithmically decreases with increasing stimulus intensity regardless of the sensory modality (Pieron, 1952). Manipulating BU target luminance decreased and then increased SRT with increasing BU target luminance in violation of this law (Marino & Munoz, 2009). The model revealed that the spatial interactions of individual BU visual signals within the SC map can produce violations of Pieron's law whenever the width of the BU point image becomes large enough to activate lateral inhibitory connections and cause SRT to increase. Thus, the interactions of BU and TD point images in the SC map resulting from local excitation and distal surrounding inhibition predict a potential neural mechanism that can account for violations of Hick's and Pieron's laws within the oculomotor system. These mechanisms may be unique within the visuo-saccadic modality and thus may not translate across other sensory modalities or nonoculomotor motor responses. Future research will be required to test these assumptions.

Intrinsic versus Extrinsic Sources of Inhibition in the SC

Previous neural field models of the SC have assumed the existence of lateral inhibition that is intrinsic to the local SC circuit that results in winner-take-all behavior (Badler & Keller, 2002; Trappenberg et al., 2001; Arai, Das, Keller, & Aiyoshi, 1999; Bozis & Moschovakis, 1998; Grossberg, Roberts, Aguilar, & Bullock, 1997; Massone & Khoshaba, 1995; van Opstal & van Gisbergen, 1989). This assumption was initially supported by evidence from an in vivo electrical stimulation study (Munoz & Istvan, 1998) and an in vitro pharmacological study (Meredith & Ramoa, 1998) that showed evidence of long-range inhibitory connections in the SC. However, later evidence from in vitro slices cut across the SC lamina (parasaggital or coronal) only showed evidence for restricted, short-range inhibition (Lee & Hall, 2006). Furthermore, an in vivo microinjection study in the SC (cholinergic agonist nicotine) did not produce long range inhibitory effects on saccade performance (Watanabe, Kobayashi, Inoue, & Isa, 2005). This led Arai and Keller (2005) to eliminate all intrinsic lateral inhibition from their SC model and instead relied entirely on extrinsic lateral inhibition that was input into their model. This external inhibition was assumed to originate from the substantia nigra pars reticulata, a BG output structure that projects GABAergic inhibition into the SCi (Hikosaka, 2007). More recently, studies have provided evidence for long-range lateral interactions within the SCi, first, from an in vivo SC study that presented proximal and distal visual targets and distractors to awake behaving monkeys performing visually triggered saccades (Dorris et al., 2007). This study demonstrated spatially dependent lateral interactions (local excitation and distal inhibition) between targets and distractors; however, this study could not dissociate between intrinsic and extrinsic sources of lateral inhibition. A recent in vitro study of novel horizontal slice preparations of mouse SCi (which preserved the lateral circuitry across SCi map) has demonstrated long-range lateral inhibitory and excitatory synaptic connections that were intrinsic to the SCi when isolated by the voltage clamp technique at 0 and −80 mV (Phongphanee et al., 2008). However, unlike the superficial SC where such long-range inhibition is strong enough to distally inhibit the surrounding map, the intrinsic inhibition in the SCi is relatively weak and largely masked by local excitation (Phongphanee et al., 2008). Thus additional extrinsic inhibitory input from areas such as the BG (Hikosaka, 2007) and superficial SC (Isa & Hall, 2009) are likely required to shape the lateral interactions within the SCi map. On the basis of this evidence, we assume that the combination of these extrinsic and intrinsic sources of lateral inhibition in the SC circuitry can result in the winner-take-all behavior that we have modeled.

The lateral interactions in our model were a simplified combination of both the intrinsic (originating within the SCi) and extrinsic inhibitory signals. We acknowledge that the interactions between these two types of inhibition are likely more complex as the relative levels of each could be modulated by differing amounts of dynamic BU- and TD-related inhibition from multiple external structures, including the BG, in addition to the activity dependent inhibition from within the SC itself. However, such interactions (wherever they are) can be utilized within an organized neural field to explain the different and apparently contradictory behavioral findings previously reported. This highlights the potential power and versatility of such

simplified principles of lateral competition within a neural winner-take-all mechanism.

Acknowledgments

We thank Ann Lablans, Rebecca Cranham, Ray Pengelly, Sean Hickman, and Fred Paquin for outstanding technical assistance and the members of the Munoz laboratory for their comments on earlier versions of the manuscript. This work was funded by a research grant from the Canadian Institutes of Health Research to D. P. M. (MOP-77734). R. A. M. was supported by graduate fellowships from Queen's University, and D. P. M. was supported by the Canada Research Chair Program.

Reprint requests should be sent to Douglas P. Munoz, Centre for Neuroscience Studies, Queen's University, Kingston, Ontario, Canada K7L 3N6, or via e-mail: doug_munoz@biomed.queensu.ca.

REFERENCES

Amari, S. (1977). Dynamics of pattern formation in lateral-inhibition type neural fields. *Biological Cybernetics, 27,* 77–87.

Anderson, R. W., Keller, E. L., Gandhi, N. J., & Das, S. (1998). Two-dimensional saccade-related population activity in superior colliculus in monkey. *Journal of Neurophysiology, 80,* 798–817.

Arai, K., Das, S., Keller, E. L., & Aiyoshi, E. (1999). A distributed model of the saccade system: Simulations of temporally perturbed saccades using position and velocity feedback. *Neural Networks, 12,* 1359–1375.

Arai, K., & Keller, E. L. (2005). A model of the saccade-generating system that accounts for trajectory variations produced by competing visual stimuli. *Biological Cybernetics, 92,* 21–37.

Arai, K., McPeek, R. M., & Keller, E. L. (2004). Properties of saccadic responses in monkey when multiple competing visual stimuli are present. *Journal of Neurophysiology, 91,* 890–900.

Badler, J. B., & Keller, E. L. (2002). Decoding of a motor command vector from distributed activity in superior colliculus. *Biological Cybernetics, 86,* 179–189.

Balan, P. F., Oristaglio, J., Schneider, D. M., & Gottlieb, J. (2008). Neuronal correlates of the set-size effect in monkey lateral intraparietal area. *PLoS Biology, 6,* e158.

Basso, M. A., & Wurtz, R. H. (1998). Modulation of neuronal activity in superior colliculus by changes in target probability. *The Journal of Neuroscience, 18,* 7519–7534.

Bell, A. H., Meredith, M. A., Van Opstal, A. J., & Munoz, D. P. (2006). Stimulus intensity modifies saccadic reaction time and visual response latency in the superior colliculus. *Experimental Brain Research, 174,* 53–59.

Boch, R., Fischer, B., & Ramsperger, E. (1984). Express-saccades of the monkey: Reaction times versus intensity, size, duration, and eccentricity of their targets. *Experimental Brain Research, 55,* 223–231.

Bozis, A., & Moschovakis, A. K. (1998). Neural network simulations of the primate oculomotor system. III. An one-dimensional, one-directional model of the superior colliculus. *Biological Cybernetics, 79,* 215–230.

Bravo, M. J., & Nakayama, K. (1992). The role of attention in different visual-search tasks. *Perception & Psychophysics, 51,* 465–472.

Carpenter, R. H. (2004). Contrast, probability, and saccadic latency; evidence for independence of detection and decision. *Current Biology, 14,* 1576–1580.

Carpenter, R. H., & McDonald, S. A. (2007). LATER predicts saccade latency distributions in reading. *Experimental Brain Research, 177,* 176–183.

Carpenter, R. H., & Williams, M. L. (1995). Neural computation of log likelihood in control of saccadic eye movements. *Nature, 377,* 59–62.

Carrasco, M., & Yeshurun, Y. (1998). The contribution of covert attention to the set-size and eccentricity effects in visual search. *Journal of Experimental Psychology: Human Perception and Performance, 24,* 673–692.

Cohen, J. Y., Heitz, R. P., Woodman, G. F., & Schall, J. D. (2009). Neural basis of the set-size effect in frontal eye field: Timing of attention during visual search. *Journal of Neurophysiology, 101,* 1699–1704.

Cynader, M., & Berman, N. (1972). Receptive-field organization of monkey superior colliculus. *Journal of Neurophysiology, 35,* 187–201.

de Boore, C. (Ed.) (1978). *A practical guide to splines*. New York: Springer-Verlag.

Doma, H., & Hallett, P. E. (1988). Dependence of saccadic eye-movements on stimulus luminance, and an effect of task. *Vision Research, 28,* 915–924.

Dorris, M. C., & Munoz, D. P. (1995). A neural correlate for the gap effect on saccadic reaction times in monkey. *Journal of Neurophysiology, 73,* 2558–2562.

Dorris, M. C., & Munoz, D. P. (1998). Saccadic probability influences motor preparation signals and time to saccadic initiation. *The Journal of Neuroscience, 18,* 7015–7026.

Dorris, M. C., Olivier, E., & Munoz, D. P. (2007). Competitive integration of visual and preparatory signals in the superior colliculus during saccadic programming. *The Journal of Neuroscience, 27,* 5053–5062.

Dorris, M. C., Pare, M., & Munoz, D. P. (1997). Neuronal activity in monkey superior colliculus related to the initiation of saccadic eye movements. *The Journal of Neuroscience, 17,* 8566–8579.

Edelman, J. A., & Keller, E. L. (1998). Dependence on target configuration of express saccade-related activity in the primate superior colliculus. *Journal of Neurophysiology, 80,* 1407–1426.

Everling, S., & Munoz, D. P. (2000). Neuronal correlates for preparatory set associated with pro-saccades and anti-saccades in the primate frontal eye field. *The Journal of Neuroscience, 20,* 387–400.

Fecteau, J. H., & Munoz, D. P. (2006). Salience, relevance, and firing: A priority map for target selection. *Trends in Cognitive Sciences, 10,* 382–390.

Fischer, B. (1986). Express saccades in man and monkey. *Progress in Brain Research, 64,* 155–160.

Goldberg, M. E., & Wurtz, R. H. (1972). Activity of superior colliculus in behaving monkey. I. Visual receptive fields of single neurons. *Journal of Neurophysiology, 35,* 542–559.

Grossberg, S., Roberts, K., Aguilar, M., & Bullock, D. (1997). A neural model of multimodal adaptive saccadic eye movement control by superior colliculus. *The Journal of Neuroscience, 17,* 9706–9725.

Hall, W. C., & Moschovakis, A. K. (Eds.) (2003). *The superior colliculus: New approaches for studying sensorimotor integration*. Boca Raton, FL: CRC Press.

Hanes, D. P., & Schall, J. D. (1996). Neural control of voluntary movement initiation. *Science, 274,* 427–430.

Hays, A., Richmond, B., & Optican, L. (1982). A UNIX-based multiple process system for real-time data acquisition and control. *WESCON Conference Proceedings, 2,* 1–10.

Hick, W. E. (1952). On the rate of gain of information. *Quarterly Journal of Experimental Psychology, 4,* 11–26.

Hikosaka, O. (2007). GABAergic output of the basal ganglia. *Progress in Brain Research, 160,* 209–226.

Hubel, D. H., & Wiesel, T. N. (1969). Anatomical demonstration of columns in the monkey striate cortex. *Nature, 221,* 747–750.

Isa, T., & Hall, W. C. (2009). Exploring the superior colliculus in vitro. *Journal of Neurophysiology, 102,* 2581–2593.

Itti, L., Rees, G., & Tsotsos, J. K. (2005). *Neurobiology of attention*. San Diego, CA: Elsevier.

Jaskowski, P., & Sobieralska, K. (2004). Effect of stimulus intensity on manual and saccadic reaction time. *Perception & Psychophysics, 66,* 535–544.

Kaas, J. H. (1997). Topographic maps are fundamental to sensory processing. *Brain Research Bulletin, 44,* 107–112.

Kopecz, K. (1995). Saccadic reaction times in gap/overlap paradigms: A model based on integration of intentional and visual information on neural, dynamic fields. *Vision Research, 35,* 2911–2925.

Kopecz, K., & Schoner, G. (1995). Saccadic motor planning by integrating visual information and pre-information on neural dynamic fields. *Biological Cybernetics, 73,* 49–60.

Krauzlis, R. J. (2003). Neuronal activity in the rostral superior colliculus related to the initiation of pursuit and saccadic eye movements. *The Journal of Neuroscience, 23,* 4333–4344.

Kveraga, K., Boucher, L., & Hughes, H. C. (2002). Saccades operate in violation of Hick's law. *Experimental Brain Research, 146,* 307–314.

Kveraga, K., & Hughes, H. C. (2005). Effects of stimulus-response uncertainty on saccades to near-threshold targets. *Experimental Brain Research, 162,* 401–405.

Lawrence, B. M., St John, A., Abrams, R. A., & Snyder, L. H. (2008). An anti-Hick's effect in monkey and human saccade reaction times. *Journal of Vision, 8,* 26.1–26.7.

Lee, K. M., Keller, E. L., & Heinen, S. J. (2005). Properties of saccades generated as a choice response. *Experimental Brain Research, 162,* 278–286.

Lee, P., & Hall, W. C. (2006). An in vitro study of horizontal connections in the intermediate layer of the superior colliculus. *Journal of Neuroscience, 26,* 4763–4768.

Li, X., & Basso, M. A. (2008). Preparing to move increases the sensitivity of superior colliculus neurons. *The Journal of Neuroscience, 28,* 4561–4577.

Ludwig, C. J., Gilchrist, I. D., & McSorley, E. (2004). The influence of spatial frequency and contrast on saccade latencies. *Vision Research, 44,* 2597–2604.

Machado, L., & Rafal, R. D. (2000). Strategic control over saccadic eye movements: Studies of the fixation offset effect. *Perception & Psychophysics, 62,* 1236–1242.

Marino, R. A., Levy, R., Boehnke, S., White, B. J., Itti, L., & Munoz, D. P. (in revision). Linking visual response properties in the superior colliculus to saccade behavior.

Marino, R. A., & Munoz, D. P. (2009). The effects of bottom–up target luminance and top–down spatial target predictability on saccadic reaction times. *Experimental Brain Research, 197,* 321–335.

Marino, R. A., Rodgers, C. K., Levy, R., & Munoz, D. P. (2008). Spatial relationships of visuomotor transformations in the superior colliculus map. *Journal of Neurophysiology, 100,* 2564–2576.

Massone, L. L. E., & Khoshaba, T. (1995). Local dynamic interactions in the collicular motor map: A neural network model. *Network: Computation in Neural Systems, 6,* 1–18.

McIlwain, J. T. (1975). Visual receptive fields and their images in superior colliculus of the cat. *Journal of Neurophysiology, 38,* 219–230.

McIlwain, J. T. (1986). Point images in the visual system: New interest in an old idea. *Trends in Neurosciences, 9,* 354.

McPeek, R. M., & Keller, E. L. (2001). Short-term priming, concurrent processing, and saccade curvature during a target selection task in the monkey. *Vision Research, 41,* 785–800.

McPeek, R. M., & Keller, E. L. (2002). Saccade target selection in the superior colliculus during a visual search task. *Journal of Neurophysiology, 88,* 2019–2034.

McPeek, R. M., Maljkovic, V., & Nakayama, K. (1999). Saccades require focal attention and are facilitated by a short-term memory system. *Vision Research, 39,* 1555–1566.

McPeek, R. M., & Schiller, P. H. (1994). The effects of visual scene composition on the latency of saccadic eye movements of the rhesus monkey. *Vision Research, 34,* 2293–2305.

Meredith, M. A., & Ramoa, A. S. (1998). Intrinsic circuitry of the superior colliculus: Pharmacophysiological identification of horizontally oriented inhibitory interneurons. *Journal of Neurophysiology, 79,* 1597–1602.

Meredith, M. A., & Stein, B. E. (1985). Descending efferents from the superior colliculus relay integrated multisensory information. *Science, 227,* 657–659.

Moschovakis, A. K., Karabelas, A. B., & Highstein, S. M. (1988). Structure–function relationships in the primate superior colliculus: II. Morphological identity of presaccadic neurons. *Journal of Neurophysiology, 60,* 263–302.

Munoz, D. P., & Fecteau, J. H. (2002). Vying for dominance: Dynamic interactions control visual fixation and saccadic initiation in the superior colliculus. *Progress in Brain Research, 140,* 3–19.

Munoz, D. P., & Istvan, P. J. (1998). Lateral inhibitory interactions in the intermediate layers of the monkey superior colliculus. *Journal of Neurophysiology, 79,* 1193–1209.

Munoz, D. P., & Schall, J. D. (2003). Concurrent, distributed control of saccade initiation in the frontal eye field and superior colliculus. In W. C. Hall & A. Moschovakis (Eds.), *The superior colliculus: New approaches for studying sensorimotor integration* (p. 55). Boca Raton, FL: CRC Press.

Munoz, D. P., & Wurtz, R. H. (1993). Fixation cells in monkey superior colliculus: I. Characteristics of cell discharge. *Journal of Neurophysiology, 70,* 559–575.

Munoz, D. P., & Wurtz, R. H. (1995a). Saccade-related activity in monkey superior colliculus: I. Characteristics of burst and buildup cells. *Journal of Neurophysiology, 73,* 2313–2333.

Munoz, D. P., & Wurtz, R. H. (1995b). Saccade-related activity in monkey superior colliculus: II. Spread of activity during saccades. *Journal of Neurophysiology, 73,* 2334–2348.

Ottes, F. P., Van Gisbergen, J. A., & Eggermont, J. J. (1986). Visuomotor fields of the superior colliculus: A quantitative model. *Vision Research, 26,* 857–873.

Paré, M., & Hanes, D. P. (2003). Controlled movement processing: Superior colliculus activity associated with countermanded saccades. *The Journal of Neuroscience, 23,* 6480–6489.

Paré, M., & Munoz, D. P. (1996). Saccadic reaction time in the monkey: Advanced preparation of oculomotor programs is primarily responsible for express saccade occurrence. *Journal of Neurophysiology, 76,* 3666–3681.

Perry, V. H., & Cowey, A. (1985). The ganglion cell and cone distributions in the monkey's retina: Implications for central magnification factors. *Vision Research, 25,* 1795–1810.

Phongphanee, P., Marino, R. A., Kaneda, K., Yanagawa, Y., Munoz, D. P., & Isa, T. (2008). The lateral interaction in the superficial and intermediate layers of the mouse superior colliculus slice [Abstract]. *Society for Neuroscience Abstracts,* 167.17.

Pieron, H. (1952). *The sensations: Their functions, processes and mechanisms*. London: Frederick Muller Ltd.

Posner, M. I. (2005). Timing the brain: Mental chronometry as a tool in neuroscience. *PLoS Biology, 3,* e51.

Reddi, B. A., Asrress, K. N., & Carpenter, R. H. (2003). Accuracy, information, and response time in a saccadic decision task. *Journal of Neurophysiology, 90,* 3538–3546.
Reddi, B. A., & Carpenter, R. H. (2000). The influence of urgency on decision time. *Nature Neuroscience, 3,* 827–830.
Richmond, B. J., Optican, L. M., Podell, M., & Spitzer, H. (1987). Temporal encoding of two-dimensional patterns by single units in primate inferior temporal cortex. I. Response characteristics. *Journal of Neurophysiology, 57,* 132–146.
Robinson, D. A. (1972). Eye movements evoked by collicular stimulation in the alert monkey. *Vision Research, 12,* 1795–1808.
Rodgers, C. K., Munoz, D. P., Scott, S. H., & Pare, M. (2006). Discharge properties of monkey tectoreticular neurons. *Journal of Neurophysiology, 95,* 3502–3511.
Saslow, M. G. (1967). Effects of components of displacement-step stimuli upon latency for saccadic eye movement. *Journal of the Optical Society of America, 57,* 1024–1029.
Schall, J. D. (1995). Neural basis of saccade target selection. *Reviews in the Neurosciences, 6,* 63–85.
Schall, J. D., & Thompson, K. G. (1999). Neural selection and control of visually guided eye movements. *Annual Review of Neuroscience, 22,* 241–259.
Schiller, P. H., Sandell, J. H., & Maunsell, J. H. (1987). The effect of frontal eye field and superior colliculus lesions on saccadic latencies in the rhesus monkey. *Journal of Neurophysiology, 57,* 1033–1049.
Schiller, P. H., True, S. D., & Conway, J. L. (1980). Deficits in eye movements following frontal eye-field and superior colliculus ablations. *Journal of Neurophysiology, 44,* 1175–1189.
Scudder, C. A., Moschovakis, A. K., Karabelas, A. B., & Highstein, S. M. (1996). Anatomy and physiology of saccadic long-lead burst neurons recorded in the alert squirrel monkey. I. Descending projections from the mesencephalon. *Journal of Neurophysiology, 76,* 332–352.
Shen, K., & Pare, M. (2006). Guidance of eye movements during visual conjunction search: Local and global contextual effects on target discriminability. *Journal of Neurophysiology, 95,* 2845–2855.
Sinha, N., Brown, J. T., & Carpenter, R. H. (2006). Task switching as a two-stage decision process. *Journal of Neurophysiology, 95,* 3146–3153.
Sparks, D. L. (1978). Functional properties of neurons in the monkey superior colliculus: Coupling of neuronal activity and saccade onset. *Brain Research, 156,* 1–16.
Sparks, D. L., & Hartwich-Young, R. (1989). The deep layers of the superior colliculus. *Reviews of Oculomotor Research, 3,* 213–255.
Sparks, D. L., & Mays, L. E. (1980). Movement fields of saccade-related burst neurons in the monkey superior colliculus. *Brain Research, 190,* 39–50.
Story, G. W., & Carpenter, R. H. (2009). Dual LATER-unit model predicts saccadic reaction time distributions in gap, step and appearance tasks. *Experimental Brain Research. Experimentelle Hirnforschung. Experimentation Cerebrale, 193,* 287–296.
Thiem, P. D., Hill, J. A., Lee, K. M., & Keller, E. L. (2008). Behavioral properties of saccades generated as a choice response. *Experimental Brain Research, 186,* 355–364.
Trappenberg, T. P. (2008). Decision making and population decoding with strongly inhibitory neural field models. In D. Heinke & E. Mavritsaki (Eds.), *Computational modelling in behavioural neuroscience: Closing the gap between neurophysiology and behaviour*. London: Psychology Press.
Trappenberg, T. P., Dorris, M. C., Munoz, D. P., & Klein, R. M. (2001). A model of saccade initiation based on the competitive integration of exogenous and endogenous signals in the superior colliculus. *Journal of Cognitive Neuroscience, 13,* 256–271.
Van Gisbergen, J. A., Van Opstal, A. J., & Tax, A. A. (1987). Collicular ensemble coding of saccades based on vector summation. *Neuroscience, 21,* 541–555.
van Opstal, A. J., & van Gisbergen, J. A. M. (1989). Scatter in the metrics of saccades and properties of the collicular motor map. *Vision Research, 29,* 1183–1196.
Wang, X., Jin, J., & Jabri, M. (2002). Neural network models for the gaze shift system in the superior colliculus and cerebellum. *Neural Networks, 15,* 811–832.
Watanabe, M., Kobayashi, Y., Inoue, Y., & Isa, T. (2005). Effects of local nicotinic activation of the superior colliculus on saccades in monkeys. *Journal of Neurophysiology, 93,* 519–534.
White, B. J., Kerzel, D., & Gegenfurtner, K. R. (2006). Visually guided movements to color targets. *Experimental Brain Research, 175,* 110–126.